

SURFACE SEPARATION AND CONTACT RESISTANCE CONSIDERING
SINUSOIDAL ELASTIC-PLASTIC MULTISCALE ROUGH
SURFACE CONTACT

Except where reference is made to the work of others, the work described in this thesis is my own or was done in collaboration with my advisory committee. This thesis does not include proprietary or classified information.

William Everett Wilson

Certificate of Approval:

George T. Flowers
Professor
Mechanical Engineering

Robert L. Jackson, Chair
Assistant Professor
Mechanical Engineering

Dan B. Marghitu
Professor
Mechanical Engineering

George T. Flowers
Dean
Graduate School

SURFACE SEPARATION AND CONTACT RESISTANCE CONSIDERING
SINUSOIDAL ELASTIC-PLASTIC MULTISCALE ROUGH
SURFACE CONTACT

W. Everett Wilson

A Thesis

Submitted to

the Graduate Faculty of

Auburn University

in Partial Fulfillment of the

Requirements for the

Degree of

Master of Science

Auburn, Alabama
December 19, 2008

SURFACE SEPARATION AND CONTACT RESISTANCE CONSIDERING
SINUSOIDAL ELASTIC-PLASTIC MULTISCALE ROUGH
SURFACE CONTACT

William Everett Wilson

Permission is granted to Auburn University to make copies of this thesis at its discretion, upon the request of individuals or institutions and at their expense. The author reserves all publication rights.

Signature of Author

Date of Graduation

VITA

W. Everett Wilson, son of Jim and Betty Wilson was born on August 22, 1984, in Birmingham, Alabama. He graduated high school from Gardendale High School, Gardendale, Alabama in May 2002. He attended Troy University, Troy, Alabama and graduated in May 2006 with the degree of Bachelor of Science in Mathematics, minoring in Business Administration. He joined the Masters program in the department of Mechanical Engineering at Auburn University in August 2006.

THESIS ABSTRACT

SURFACE SEPARATION AND CONTACT RESISTANCE CONSIDERING

SINUSOIDAL ELASTIC-PLASTIC MULTISCALE ROUGH

SURFACE CONTACT

W. Everett Wilson

Master of Science, December 19, 2008
(B.S., Troy University, 2006)

95 Typed Pages

Directed by Robert L. Jackson

This thesis considers the multiscale nature of surface roughness in a new model that predicts the real area of contact and surface separation as functions of load. This work is based upon a previous rough surface multiscale contact model which used stacked elastic-plastic spheres to model the multiple scales of roughness. Instead, this work uses stacked 3-D sinusoids to represent the asperities in contact at each scale of the surface. By summing the distance between the two surfaces at all scales, a model of surface separation as a function of dimensionless load is obtained. Since the model makes predictions for the real area of contact, it is also able to make predictions for thermal and electrical contact resistance. For the specific case of thermal contact resistance, scale-dependent surface characteristics are taken into account in this model.

In the field of contact mechanics, concern has been voiced that the iterative calculation of the real contact area in multiscale methods does not converge. This issue has been addressed with results not only confirming convergence but also giving the conditions necessary for the sinusoidal based multiscale method to converge.

To further verify the results of this new method, all results and calculations are compared to previous works that were based upon statistical mathematics to model contact area and load. These comparisons have given qualitative support to the sinusoidal multiscale technique featured here as well as revealing some possible shortcomings of the statistical techniques, particularly in the area of surface separation calculations. Upon further investigation, a correction is proposed in this work that alleviates this short-coming for statistical contact modeling. The multiscale sinusoidal based elastic-plastic modeling technique is calculated and compared for a variety of surfaces, each with a differing roughness with appropriate results. Finally, in an effort to experimentally validate the electrical contact resistance theoretical results, the initial setup and outline behind an experimental test rig is explained.

ACKNOWLEDGEMENTS

The time I spent at Auburn University studying with the goal of obtaining a Master's Degree in Mechanical Engineering would have seen much less success without the excellent guidance I received along the way. The credit for that goes primarily to Dr. Robert L. Jackson who provided me with the opportunity and means to study at this esteemed university but also served as a diligent mentor, director, professor, and friend along the way. His assistance and encouragement to constantly expand my efforts and overcome my obstacles has been a deeply rewarding experience. Special thanks also go to Dr. George T. Flowers and Dr. Dan B. Marghitu for serving on my graduate committee. The faculty and staff of the Mechanical Engineering Department at Auburn University also deserve recognition for their services provided throughout my graduate student years. I would also like to thank Santosh Angadi, Jeremy Dawkins, Vijaykumar Krithivasan, and Saurabh Wadwalkar for their friendship and many shared laughs and frustrations in the Multiscale Tribology Laboratory at Auburn University.

Without a doubt, the most influential people in my life have been my loving parents, Jim and Betty Wilson. They have constantly told me of their dreams of success for me and ensured I was aware of their pride in me and that support and love has been invincible in my life's quests and journeys.

Style manual or journal used Guide to Preparation and Submission of Theses and
Dissertations and Bibliography as per ASME

Computer software used Microsoft Office 2003, Matlab 7.0.4

TABLE OF CONTENTS

LIST OF FIGURES	ix	
LIST OF TABLES	xii	
NOMENCLATURE	xiii	
1	INTRODUCTION	1
2	BACKGROUND	3
	2.1 Introduction	3
	2.2 Statistical Models	3
	2.3 Fractal Models	5
	2.4 Multiscale Models	7
3	OBJECTIVES	10
4	METHODOLOGY	12
	4.1 Introduction	12
	4.2 Multiscale Sinusoidal Perfectly Elastic Contact	12
	4.3 Multiscale Sinusoidal Elastic-Plastic Contact	16
	4.4 Statistical Perfectly Elastic Contact	18
	4.5 Statistical Elastic-Plastic Contact	21
	4.6 Electrical Contact Resistance	22
	4.6.1 Multiscale Electrical Contact Resistance	23
	4.6.2 Statistical Electrical Contact Resistance	25
	4.7 Thermal Contact Resistance	26
	4.8 Scale Dependent Thermal Contact Resistance	27
	4.9 Convergence of Real Area of Contact	28
	4.10 Adjusted Statistical Surface Separation	29
5	EXPERIMENTAL DESIGN	31
6	RESULTS	34
	6.1 Introduction	34
	6.2 Convergence of Real Area of Contact	35
	6.3 Contact Resistance Model Comparison	39

6.3.1	Calculated Real Area of Contact	41
6.3.2	Surface Separation	42
6.3.3	Electrical Contact Resistance	45
6.3.4	Thermal Contact Resistance	47
6.4	Comparison between Multiple Surfaces	48
6.4.1	Calculated Real Area of Contact	50
6.4.2	Surface Separation	55
6.4.3	Electrical Contact Resistance	64
6.4.4	Thermal Contact Resistance	69
7	CONCLUSIONS	75
	BIBLIOGRAPHY	77

LIST OF FIGURES

1.1	A schematic depicting the decomposition of a surface into superimposed sine waves.	1
2.1	Spherical contact model before contact (a), during mostly elastic deformation (b), and during mostly plastic deformation (c).	4
4.1	Graphical explanation of common terms used for the sinusoidal based multiscale contact model.	13
4.2	Graphic depicting comparison of JGH asymptotic solutions with Eq. (4.10).	16
4.3	Schematic of “bottlenecked” current flow through asperities.	23
4.4	Graphical comparison of surface separation and adjusted surface separation.	29
5.1	Schematic of electrical contact resistance test apparatus.	32
6.1	Contact area ratio as a function of wavelength for perfectly elastic multiscale method where α is varied in Eq. (31).	35
6.2	Contact area ratio as a function of wavelength for elastic-plastic multiscale method where α is varied in Eq. (4.53).	36
6.3	Contact area ratio as a function of wavelength for perfectly elastic multiscale method where γ is varied in Eq. (4.53).	37
6.4	Contact area ratio as a function of wavelength for elastic-plastic multiscale method where γ is varied in Eq. (4.53).	38
6.5	Non-dimensional area vs. load.	41
6.6	Area compared to Surface Separation including the adjusted separation for Statistical Contact Methods.	42
6.7	Non-dimensional surface separation vs. load.	44

6.8	Electrical contact resistance as a function of non-dimensional load.	45
6.9	Thermal contact resistance as a function of non-dimensional load including scale-dependent results.	47
6.10	Surface profile data with different roughness values.	49
6.11	Real area of contact as a function of dimensionless load for surfaces of different roughness modeled using the sinusoidal based multiscale method for elastic-plastic material deformation.	51
6.12	Real area of contact as a function of dimensionless load for surfaces of different roughness modeled using the sinusoidal based multiscale method for perfectly elastic material deformation.	52
6.13	Real area of contact as a function of dimensionless load for surfaces of different roughness modeled using the JG statistical method for elastic-plastic material deformation.	53
6.14	Real area of contact as a function of dimensionless load for surfaces of different roughness modeled using the GW statistical method for perfectly elastic material deformation.	54
6.15	Surface Separation as a function of dimensionless load for surfaces of different roughness modeled using the sinusoidal based multiscale method for elastic-plastic material deformation.	56
6.16	Surface Separation as a function of dimensionless load for surfaces of different roughness modeled using the sinusoidal based multiscale method for perfectly elastic material deformation.	57
6.17	Surface Separation as a function of dimensionless load for surfaces of different roughness modeled using the JG statistical method for elastic-plastic material deformation.	58
6.18	Surface Separation as a function of dimensionless load for surfaces of different roughness modeled using the GW statistical method for perfectly elastic material deformation.	59
6.19	Surface separation as a function of real area of contact for surfaces of different roughness modeled using the sinusoidal based multiscale method for elastic-plastic material deformation.	60

6.20	Surface separation as a function of real area of contact for surfaces of different roughness modeled using the sinusoidal based multiscale method for perfectly elastic material deformation.	61
6.21	Surface separation as a function of real area of contact for surfaces of different roughness modeled using the JG statistical method for elastic-plastic material deformation.	62
6.22	Surface separation as a function of real area of contact for surfaces of different roughness modeled using the GW statistical method for perfectly elastic material deformation.	63
6.23	Electrical contact resistance (ECR) as a function of dimensionless load for surfaces of different roughness modeled using the sinusoidal based multiscale method for elastic-plastic material deformation.	65
6.24	Electrical contact resistance (ECR) as a function of dimensionless load for surfaces of different roughness modeled using the sinusoidal based multiscale method for perfectly elastic material deformation.	66
6.25	Electrical contact resistance (ECR) as a function of dimensionless load for surfaces of different roughness modeled using the JG statistical method for elastic-plastic material deformation.	67
6.26	Electrical contact resistance (ECR) as a function of dimensionless load for surfaces of different roughness modeled using the GW statistical method for elastic-plastic material deformation.	68
6.27	Thermal contact resistance (TCR) as a function of dimensionless load for surfaces of different roughness modeled using the sinusoidal based multiscale method for elastic-plastic material deformation.	70
6.28	Thermal contact resistance (TCR) as a function of dimensionless load for surfaces of different roughness modeled using the sinusoidal based multiscale method for perfectly elastic material deformation.	71
6.29	Thermal contact resistance (TCR) as a function of dimensionless load for surfaces of different roughness modeled using the JG statistical method for elastic-plastic material deformation.	72
6.30	Thermal contact resistance (TCR) as a function of dimensionless load for surfaces of different roughness modeled using the GW statistical method for perfectly elastic material deformation.	73

LIST OF TABLES

6.1	Material Properties of Tin	39
6.2	Rough Surface Characteristics and Convergence Variables.	49
6.3	Rough Surface Characteristics and Adjusted Separation Values (Eq. 4.54).	63

NOMENCLATURE

A	area of contact
\bar{A}	individual asperity area of contact
A_n	nominal contact area
a	radius of the area of contact
B	material dependant exponent
C	critical yield stress coefficient
C_p	heat capacity per unit volume
D	contact area factor
d	separation of mean asperity height
E	elastic modulus
E'	$E/(1-\nu^2)$
Er	electrical contact resistance
e_y	yield strength to elastic modulus ratio, S_y / E'
F	Constant found from slope of Fourier Series
f	spatial frequency (reciprocal of wavelength)
G	asymptotic solution from JGH
H_G	geometrical hardness limit
K	hardness factor
Kn	Knudsen number
k	thermal conductivity
L	scan length
M	spectral moment of the surface
N	total number of asperities
P	contact force
\bar{P}	individual asperity contact force
p	mean pressure
p^*	average pressure for complete contact
q	elastic-plastic variable
R	radius of hemispherical asperity
S_y	yield strength
Tr	thermal contact resistance
v_s	solid speed of sound
y_s	distance between the mean asperity height and the mean surface height
z	height of asperity measured from the mean of asperity heights

Greek Symbols

A	coefficient of surface spectrum equation
γ	exponent of surface spectrum equation
η	area density of asperities
η	separation of mean surface height
σ	standard deviation of surface heights
σ_s	standard deviation of asperity heights
λ	asperity wavelength
λ_{MFP}	phonon mean free path
ρ	density of surface material
ρ_L	electrical resistivity of surface material
ρ_T	thermal resistivity of surface material
Δ	asperity amplitude
Φ	distribution function of asperity heights
ω	interference between hemisphere and surface
ν	Poisson's ratio

Subscripts

E	elastic regime
P	plastic regime
c	critical value at onset of plastic deformation
i	frequency level
JGH	from Johnson, Greenwood, and Higginson [10]
JG	from Jackson and Green [15]
asp	asperity
sur	surface
L	electrical
T	thermal
SD	scale-dependent

CHAPTER 1
INTRODUCTION

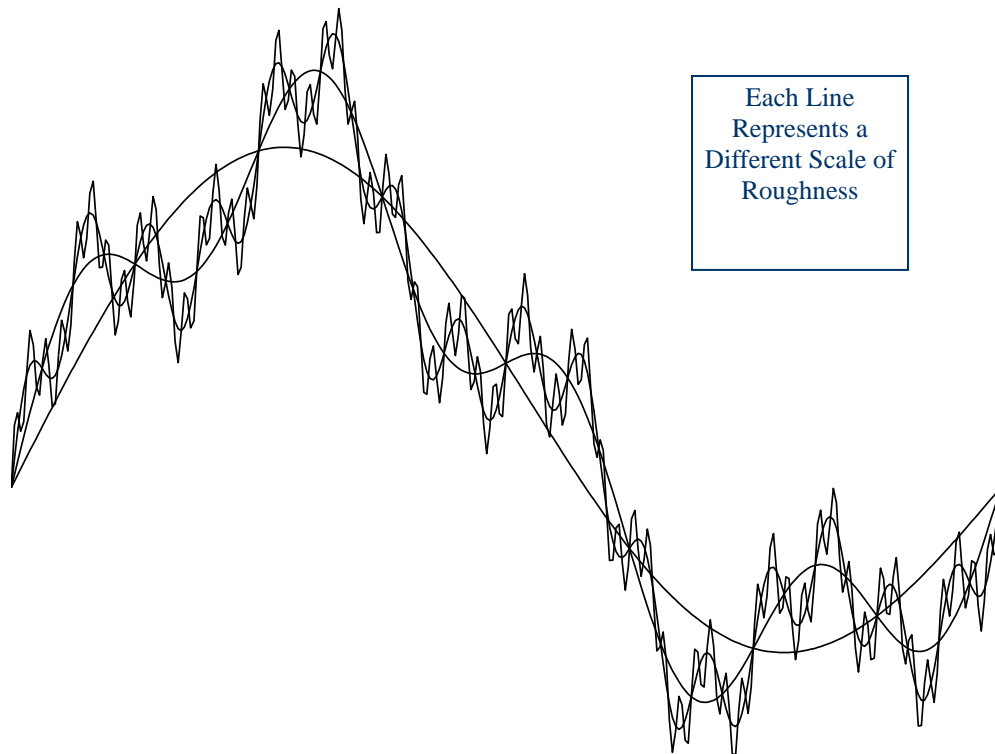


Figure 1.1: A schematic depicting the decomposition of a surface into superimposed sine waves.

There are many different methods to model the contact of rough surfaces including statistical [1-4], fractal [5-8], and multiscale models [9-11]. Statistical modeling techniques use mathematical parameters of the surface to generalize the surface

into a statistical probability to determine the amount of contact and force. The fractal mathematics based methods were derived to account for different scales of surface features not accounted for by the statistical models. The multiscale models were developed to alleviate the assumptions imposed by fractal mathematics and to also improve how the material deformation mechanics are considered. This work uses a Fourier transform to convert the data into a series of stacked sinusoids, as shown in Fig. 1.1. In a previous work [11] a method to calculate the surface separation from the multiscale model was not provided. It is in the current work. In addition, this work differs from a previous multiscale model [11] in that it uses sine shaped surfaces instead of spherical shaped surfaces to model contact of the asperities. The current work also provides a methodology for calculating the electrical and thermal contact resistance using the multiscale methodology. This provides a method for including the effect of the scale dependent thermal properties [12-16]. Also, the surface characteristics necessary to obtain convergence of the iterative multiscale scheme is examined.

CHAPTER 2

BACKGROUND

2.1 Introduction

This chapter is devoted to the background material considered in the modeling of rough surface contact, surface separation and contact resistances seen in this thesis. The first task will be to give an overview to a few of the many various contact mechanics techniques available. The primary models discussed here will include the multiscale, statistical, and fractal methods. Each of these methods is unique in its assumptions and mathematical techniques despite considerable qualitative agreement in their results. The surface separation and electrical and thermal contact resistance will be discussed later in this thesis in the methodology section.

2.2 Statistical Methods

One of the earliest works in the field of contact mechanics has been credited to Heinrich Hertz in his paper titled, *On the contact of elastic solids*, 1882. Based upon finding of interference fringes between glass lenses, his work displayed elastic displacement in surfaces that were compatible with his proposed elliptical pressure distribution. This distribution is, in fact, currently known as the Hertzian contact solution [17]. Since this finding, many models have been developed to expand the Hertzian contact solution from a single asperity or raised portion on a surface into a network of

related asperities that can more accurately describe the topography seen on engineering surfaces. One of the very popular expansion techniques is the statistical contact model.

One such statistical effort is given by Greenwood and Williamson [1]. In their work, known throughout this thesis as the GW model, the interaction between two planes is considered. One of these is a perfect flat while the other is covered in spherically shaped asperities. The primary assumptions of this model are that all the asperities must have the same radius of curvature, each asperity behaves independently of its neighbors, and the substrate material is not allowed to deform, only the asperities. With these assumptions, the contact area is determined through statistical mathematics since the asperity heights are presumed to fit a Gaussian distribution. Therefore, the Gaussian distribution gives the percentage of the surface in contact at each from the flat to the rough surface generally in terms of standard deviation. This work gives results for elastic deformation because it uses a Hertzian contact solution at the spherical tips which assumes that the surface returns to its exact original profile and shape after a loading cycle. The mathematical equations and results for this model will be given later in this thesis.

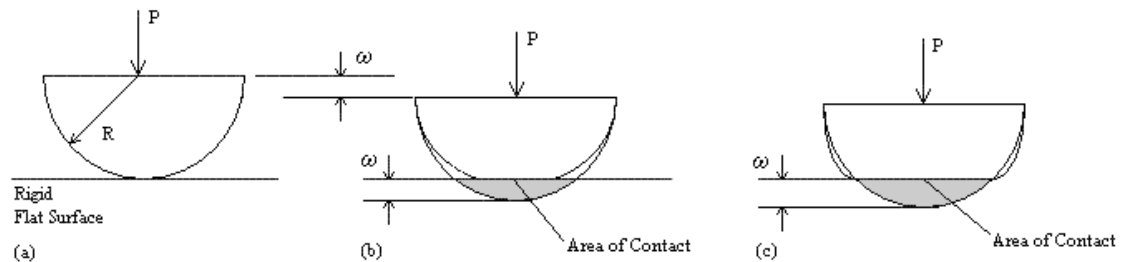


Figure 2.1: Spherical contact model before contact (a), during mostly elastic deformation (b), and during mostly plastic deformation (c).

In order to further refine the statistical model, the effects of elastic-plastic deformation have been included by numerous researchers. One such model is given by Jackson and Green (JG) [18], which establishes that the range for which the statistical model remains perfectly elastic is limited to lower loads. There are many differing models that include the effects of plasticity in statistical modeling such as those offered by Chang, Etsion, and Bogy [19] and Kogut and Etsion [20] but these methods are not considered in detail for this work. As the two surfaces increase contact pressure, the internal stresses of the asperities will eventually cause the material to yield and deform plastically. The statistical models rely on the interference value between the two surfaces which describes the amount of material that must deform for two surfaces to maintain a given separation. In other words, this is the material that would overlap if the two surfaces could pass into one another without deforming seen as the gray area in Fig. 2.1. To determine the onset of plasticity, a critical interference is calculated based upon common surface material parameters that determine when the equation formulated by GW must be altered from the Hertzian solution (perfectly elastic) to JG solution which gives elastic-plastic results. This model is based upon the assumption of the GW statistical model and is limited to relatively small deformations; the contact radius can only be 41% of the radius of curvature.

2.3 Fractal Models

The statistical models have shown to be a reliable and easily implemented technique but do have some short comings. For example, the assumptions made are essentially averaging an entire rough surface into a single radius of curvature.

Essentially, this means statistical models neglect the effects of different scales of features on a surface. Close examination of any surface shows this to be quite inaccurate since the topography of a surface in fact appears quite random. However, it is very difficult to calculate surface characteristics for a real engineering surface due to its random nature. This is the cause for the advent of the fractal modeling techniques.

The current research does not actually model a fractal technique but it is included here simply to compare with the models and assumptions made in this work. One such fractal method is Majumdar and Bhushan (MB) [21]. Through the course of their work, they found that a surface is multiscale in nature in that as a surface is viewed with a higher magnification, each new “scale” will show a topographical roughness. To assist in modeling this phenomenon, the fractal methods assume that a true rough surface appears and behaves like a mathematical fractal equation, hence their name. In the case of MB, the equation is the Weierstrass-Mandelbrot function. The fractal equation assumes self-affinity but not self-similarity. This means that each scale of the surface is related by the fractal equations but the relation is different in the normal and lateral directions. The parameters necessary for this equation are garnered from a comparison of the power spectrum fit of the rough surface data with the power spectrum of the Weierstrass-Mandelbrot function.

From this point MB calculate elastic-plastic contact mechanics through mathematical relations to the Weierstrass-Mandelbrot function and the power spectrum of the surface. This does alleviate some of the assumptions made in statistical models in that the surface parameters, specifically radius of curvature of asperities is now dependent upon the size of contact. However, it is possible that a surface may not have

an appropriate power spectrum and therefore cannot be related to the fractal equation and this model is continually self-affine with no bounds to how small a scale can be considered in this model. In addition, the MB fractal models use a very primitive contact mechanics model that basically assumes that the real area of contact can be calculated by simply truncating a surface through the fractal described surface.

2.4 Multiscale Models

Although the fractal technique is technically a multiscale modeling technique since it recognizes surface geometry at every scale available for contact, it has been singled out from the multiscale models for the reasons of its primary assumptions. The fractal models carry the self-affinity principle too far. The model has no stopping point although the physical world does. At some scale, the surface is viewed so closely that the only remaining topography is the individual molecules. Logically the scale modeling must stop around this point. There is no smaller surface characteristic to view. Also, all the scales of a surface will never be perfectly described by a single fractal equation. The multiscale models developed in this work are ideal for this situation.

The multiscale modeling technique is initiated from Archard's "protuberance upon protuberance" modeling scheme [22]. In an early multiscale non-fractal technique, Archard expanded the Hertzian sphere against flat contact to feature a sphere of a certain radius coated with hemi-spheres of another radius which are all then coated with smaller hemi-spheres of a third radius. This is the basis of a multiscale technique. Each set of spheres with their own unique radius is a "scale" and as load is increased the small scales are pressed into complete contact where the next layer begins to compress. Archard also

proved experimentally that rougher surfaces require greater loads to flatten the asperities and that the relationship between area and load approaches linearity.

One of the primary modeling techniques featured in this work is given by Jackson and Streater [11]. Their work refines the multiscale modeling technique further by developing a model more readily adaptable to real rough surfaces. This model uses a series of stacked three dimensional sinusoidal waves to describe the multiple scales of contact. The necessary assumptions for this type of model require (1) that the smaller asperities are stacked on top of larger asperities, (2) load is distributed equally over all asperities at that level, (3) all levels carry the same overall load, and (4) a smaller asperity level is not capable of extending the contact area beyond that capable of the larger scale below. Other assumptions are required for each specific model based upon the desired deformation technique such as Jackson and Streater [11] use the Johnson, Greenwood, and Higginson [23] asymptotic solutions for perfectly elastic deformation derived from their work on 3-D wavy surfaces (JGH) [23]. The JGH asymptotic solutions are given for high and low loads so Jackson and Streater [11] fit a polynomial linking equation in between to model the complete range of contact. For this modeling technique, the areal density of asperities and radius of curvature depend upon the frequency of each level of sine waves. This is done by converting the data into a series of sine waves through a discrete Fourier transform which results in a series of frequencies and amplitudes used to calculate contact area for levels of load iteratively. The JGH asymptotes and linking equation will be discussed in detail later in Chapter 4.

Finally, the above work by Jackson and Streater [11] was modified to include plasticity by Krithivasan and Jackson [24]. The framework of the perfectly elastic

sinusoidal model given by JGH [23] can be further refined to more realistically model rough surfaces by including the contact solutions found by Krithivasan and Jackson [24] in place of the asymptotes derived from Hertzian contact. The elastic-plastic solutions were found through analysis of the finite element modeling (FEM) of a three dimensional sinusoidal asperity. Similar to the JG model for statistical elastic-plastic deformation, the model remains in a perfectly elastic deformation regime until critical values are reached. The current multiscale model doesn't rely on the interference of the two surfaces for establishing contact area and load. Instead it iteratively calculates area for each load level. Therefore, the model by Krithivasan and Jackson [24] are adjusted to include the critical contact pressure or load at which the surfaces enter the elastic-plastic regime. The equations used for this and the preceding modeling techniques are discussed in detail later in this thesis work.

CHAPTER 3

OBJECTIVES

The thesis work presented here is focused on further development of the sinusoidal based multiscale contact modeling technique originally presented by Jackson and Streater [11]. In their work, Jackson and Streater developed the necessary conditions and equations to determine the theoretical real area of contact for the sinusoidal multiscale modeling method. The sinusoidal contact work was further built upon by Krithivasan and Jackson [24] to include the effects of plasticity in the individual asperity contact model. For the thesis presented here, both the models mentioned above will be employed to calculate the real area of contact, contact pressure or load, surface separation, both electrical and thermal contact resistances, and finally the effects of scale dependent material properties will be evaluated for thermal contact resistance.

In the field of contact mechanics, there exists some concern as to the validity of the multiscale modeling techniques due to the fact that, in some instances, they fail to converge. This means that certain conditions prevent the contact area from reaching a final non-zero contact area equal to the nominal or apparent area of contact. The convergence of both multiscale modeling techniques (perfectly elastic and elastic-plastic) will be examined and the necessary conditions for convergence will be compared for a variety of surface roughness. The models themselves will also be compared for four separate sets of data gathered from a stylus profilometer, each with a varying roughness.

In addition to calculating the previously mentioned surface interactions for the sinusoidal based multiscale model, this work also compares all of the features mentioned to the pre-existing and well known statistical contact models. In the case of perfectly elastic contact, the results of the sinusoidal multiscale method will be compared to that of the Greenwood and Williamson (GW) model [1]. However, the elastic-plastic deformation will be compared to the Jackson and Green model (JG) [18]. Surface separation, electrical contact resistance, thermal contact resistance, and scale dependent thermal contact resistance will be calculated from a presented statistical technique as well.

During the course of this work, a possible error is exposed for the statistical models with respect to the prediction of surface separation. The surface separation of both perfectly elastic (GW) and elastic-plastic (JG) statistical techniques does not reach zero when the calculated real area of contact is at its maximum value at complete contact. One would assume that at the maximum contact area the entire surface area available is in contact so there cannot be any separating gap between the two surfaces being forced together. To alleviate the discrepancy, an adjusted separation model will be.

Finally, an attempt will be made to further validate the theoretical models above by designing a test apparatus. The test apparatus will be used for a comparison of electrical contact resistance as a function of load. This will be accomplished by incrementally increasing the load while taking a measurement of the voltage drop across the interacting faces of two metallic surfaces at each load step. The details of these techniques are now illuminated in the following sections.

CHAPTER 4

METHODOLOGY

4.1 Introduction

This chapter describes in detail the numerical models used to calculate rough surface contact. The numerical techniques necessary for real area of contact, contact pressure or load, and surface separation are described for the unique cases of perfectly elastic and elastic-plastic deformation. Furthermore, the fundamental theory and techniques of contact resistance are discussed for both electrical and thermal contact resistance.

4.2 Multiscale Perfectly Elastic Contact

The employed multiscale model [11] uses the same direction of thought as Archard [22], but provides a method that can be easily applied to real surfaces. First a fast Fourier transform is performed on the surface profile data to predict the terms for the Fourier series describing the surface. This series describes the surface as a summation of a series of sine and cosine waves. The complex forms of the sine and cosine terms at each frequency are combined using a complex conjugate to provide the amplitude of the waveform at each scale for further calculations. Each frequency is considered a scale or layer of asperities which are stacked iteratively upon each other. In equation form these relationships are given by:

$$A = \left(\prod_{i=1}^{i_{max}} \overline{A_i \eta_i} \right) A_n \quad (4.1)$$

$$P = \overline{P_i \eta_i} A_{i-1} \quad (4.2)$$

where A is the real area of contact, η is the areal asperity density, P is the contact load, A_n is the nominal contact area, and the subscript i denotes a frequency level, with i_{max} denoting the highest frequency level considered.

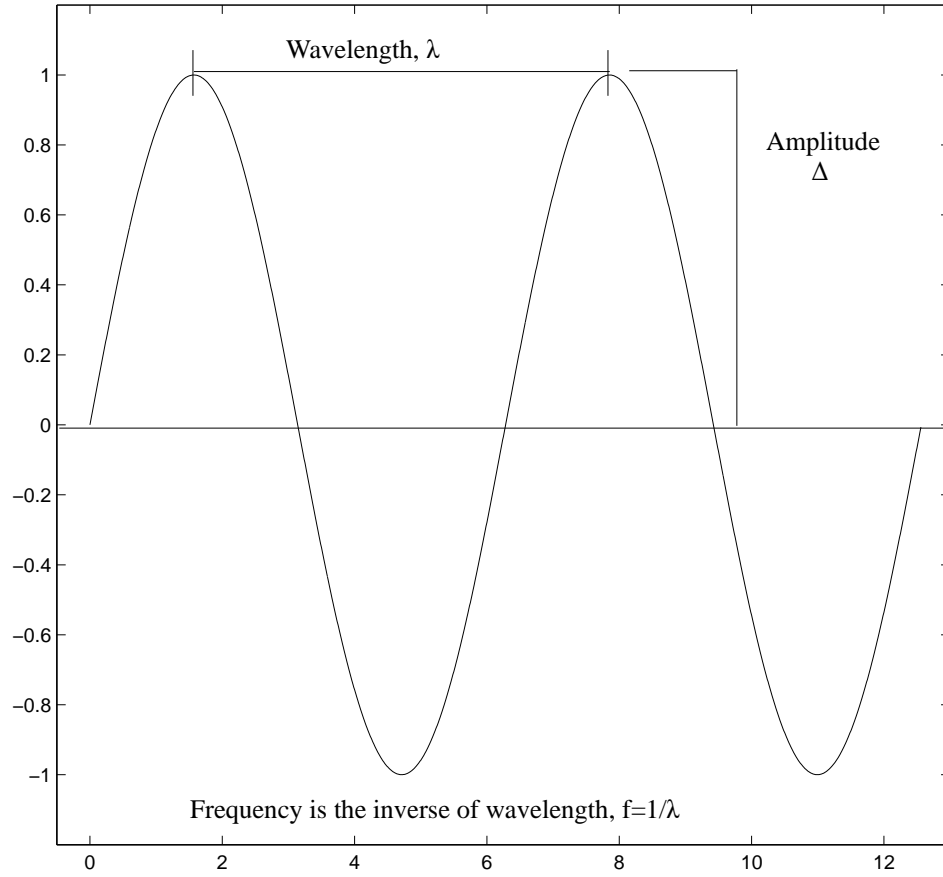


Figure 4.1: Graphical explanation of common terms used for the sinusoidal based multiscale contact model.

Each frequency level is modeled using a sinusoidal contact model. Previously derived [11] equations fit to the data and asymptotic solutions given by Johnson, Greenwood, and Higginson (JGH) [23] are used. The first equation is derived from Hertz contact and is used for low loads where $\bar{p} \ll p^*$:

$$\left(\bar{A}_{JGH}\right)_1 = \frac{2\pi}{f^2} \left[\frac{3}{8\pi} \frac{\bar{p}}{p^*} \right]^{2/3} \quad (4.3)$$

However, at higher loads where the contact is nearly complete, \bar{p} approaches p^* , and the following equation must be implemented:

$$\left(\bar{A}_{JGH}\right)_2 = \frac{1}{f^2} \left(1 - \frac{3}{2\pi} \left[1 - \frac{\bar{p}}{p^*} \right] \right) \quad (4.4)$$

Fortunately, JGH provide experimental and numerical data to support their asymptotic solutions which Jackson and Streator [11] used to fit a linking equation for the asymptotes Eq. (4.3) and Eq. (4.4) as follows:

For $\frac{\bar{p}}{p^*} < 0.8$

$$\bar{A} = \left(\bar{A}_{JGH}\right)_1 \left(1 - \left[\frac{\bar{p}}{p^*} \right]^{1.51} \right) + \left(\bar{A}_{JGH}\right)_2 \left(\frac{\bar{p}}{p^*} \right)^{1.04} \quad (4.5)$$

For $\frac{\bar{p}}{p^*} \geq 0.8$

$$\bar{A} = \left(\bar{A}_{JGH}\right)_2 \quad (4.6)$$

where p^* is the average pressure to cause complete contact between the surfaces and is given by [23] as:

$$p^* = \sqrt{2\pi E' \Delta f} \quad (4.7)$$

The current work also fits a new equation to the surface separation results given by JGH [23]. In previous works, the multiscale model was used to relate area to load. However, for many applications such as those requiring tight tolerances like sealing and lubricated bearings, it is also important to be able to predict surface separation. JGH gave asymptotic solutions for the surface separation. As $\frac{\bar{p}}{p^*}$ approaches zero, the solution is:

$$G_1 = 1 - \frac{1}{2} \left(3\pi^2 \frac{\bar{p}}{p^*} \right)^{2/3} + \left[4 \ln(\sqrt{2} + 1) \right] \cdot \left(\frac{\bar{p}}{p^*} \right) \quad (4.8)$$

While as $\frac{\bar{p}}{p^*}$ approaches 1 the solution given by [23] is:

$$G_2 = \frac{16}{15\pi^2} \left(\frac{3}{2} \right)^{3/2} \left[1 - \frac{\bar{p}}{p^*} \right]^{5/2} \quad (4.9)$$

In the current work an equation is then fit to join these two solutions:

$$\delta = \Delta \left(1 - \frac{\bar{p}}{p^*} \right) \wedge \left(0.696 \frac{\bar{p}}{p^*} + 0.158 \right) \wedge (-0.847) \quad (4.10)$$

As seen in Fig. 4.2, δ appears to be a good fit to the asymptotic functions given by Eqs. (4.8-4.9).

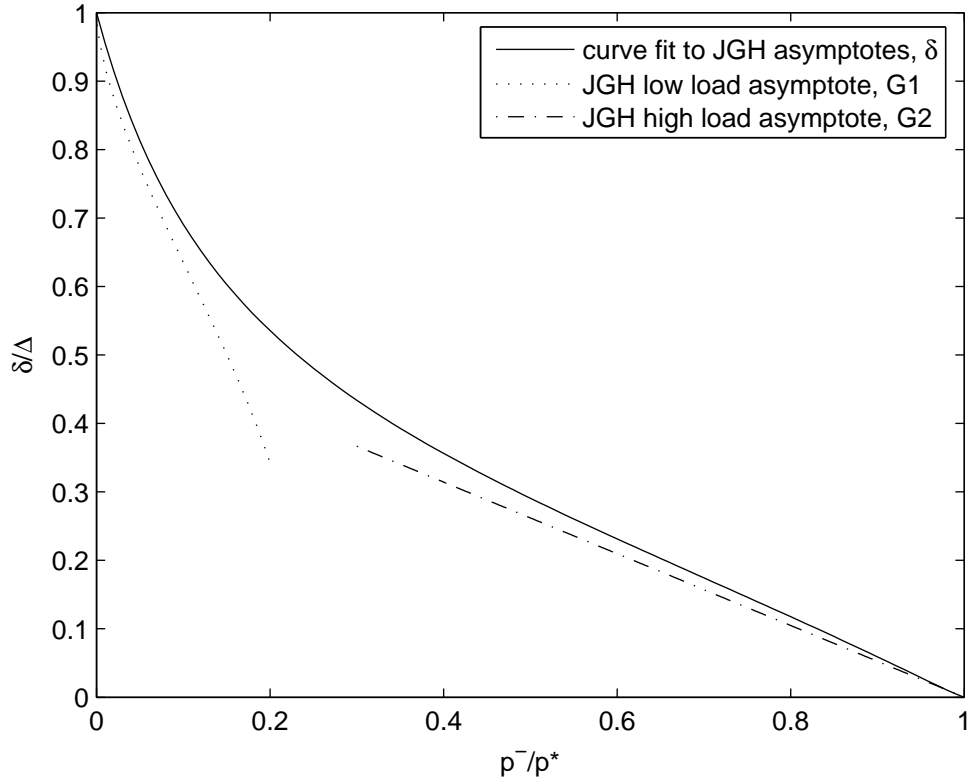


Figure 4.2: Graphic depicting comparison of JGH asymptotic solutions with Eq. (4.10).

The separation height, H , between the two surfaces is calculated by subtracting the δ value from the amplitude, Δ , at each scale level and then summing them together over all frequency scales as follows:

$$H = \sum_{i=1}^{i_{\max}} (\Delta - \delta)_i \quad (4.11)$$

4.3 Multiscale Elastic-Plastic Contact

As noted previously, many of the asperities at the different frequency levels undergo plastic deformation. Therefore an elastic-plastic sinusoidal contact model is

needed to consider this effect. The equations used in the current work to calculate the elastic-plastic contact are derived from FEM results by Krithivasan and Jackson [24] and Jackson, Krithivasan and Wilson [25]. The methodology is very similar to that of the perfectly elastic case with the exception that a different set of formulas is used once a calculated critical pressure is reached. The critical average contact pressure (P_c), critical average pressure over the nominal area (\bar{p}_c), the critical load and critical area (A_c) are given by:

$$P_c = \frac{1}{6\pi} \left(\frac{1}{\Delta f^2 E'} \right)^2 \left(\frac{C}{2} \cdot S_y \right)^3 \quad (4.12)$$

$$A_c = \frac{2}{\pi} \left(\frac{CS_y}{8\Delta f^2 E'} \right)^2 \quad (4.13)$$

$$\bar{p}_c = 2A_c P_c f^2 = 2f^2 \left(\frac{CS_y}{8\Delta f^2 E'} \right)^2 \frac{2}{\pi} \left(\frac{2CS_y}{3} \right) = \frac{1}{24\pi} \frac{(CS_y)^3}{(\Delta f E')^2} \quad (4.14)$$

where $C = 1.295 \cdot \exp(0.736\nu)$.

At low loads, $P < P_c$, and consequently small areas of contact, it is acceptable to assume that any deformation of the asperities in contact will behave perfectly elastically. However, as load increases to the critical value, plastic deformation will begin to occur within the asperities. To evaluate the plastic deformation we replace Eq. (4.3) with:

$$\bar{A}_p = 2(\bar{A}_c)^{\frac{1}{1+q}} \left(\frac{3\bar{p}}{4CS_y} \lambda^2 \right)^{\frac{q}{1+q}} \quad (4.15)$$

$$q = 3.8 \cdot \left(\frac{E'}{S_y} \cdot \frac{\Delta}{\lambda} \right)^{0.11} \quad (4.16)$$

This replacement results in the following equation for contact area:

$$\bar{A} = (\bar{A}_p) \left(1 - \left[\frac{\bar{p}}{p_p^*} \right]^{1.51} \right) + (\bar{A}_{JGH})_2 \left(\frac{\bar{p}}{p_p^*} \right)^{1.04} \quad (4.17)$$

The pressure to cause complete contact during elastic-plastic deformation is then given by [25] as:

$$\frac{p_p^*}{p^*} = \left(\frac{11}{4 \cdot \Delta / \Delta_c + 7} \right)^{3/5} \quad (4.18)$$

Where $\Delta_c = \frac{\sqrt{2} \cdot S_y \cdot \exp\left(\frac{2\nu}{3}\right)}{3\pi E' f}$ and is the critical amplitude, below which the sinusoid will

always deform in the elastic regime. Plastic deformation is caused by stress initially below the surface and building as more pressure is added. To determine the critical amplitude where plasticity begins, the maximum von Mises stress is equated to yield strength and the resulting formula solved for critical amplitude, Δ_c . Surface separation is calculated exactly as before by using Eq. (4.10), except the separation for pressures greater than \bar{p}_c must have p^* replaced by p_p^* .

4.4 Statistical Perfectly Elastic Contact

To compare and contrast the results of the multiscale sinusoidal models, statistical contact models are also calculated using the same surface parameters and profilometer results. For the perfectly elastic case, this work employs the Greenwood and Williamson [1] approach for asperity contact. The GW method requires that a few crucial assumptions be made: (1) each asperity is assumed to behave independently of

neighboring asperities, (2) all asperities have the same radius of curvature, (3) the asperity heights from the surface follow a Gaussian height distribution, and (4) only the actual asperity may deform, all substrate material is rigid as well as the contacting surface.

Using the Greenwood and Williamson [1] type statistical method hinges upon obtaining statistical parameters that describe the surface. The radius of curvature, R , and the areal asperity density, η , are calculated by McCool [26] using the spectral moments of the surfaces:

$$M_2 = \frac{1}{N} \sum_{n=1}^N \left(\frac{dz}{dx} \right)_n^2 \quad (4.19)$$

$$M_4 = \frac{1}{N} \sum_{n=1}^N \left(\frac{d^2z}{dx^2} \right)_n^2 \quad (4.20)$$

Where N is the total number of asperities on the surface and z is the distance from the mean height of the surface to the asperity peak. Then R and η are found from:

$$\eta = \left(\frac{M_4}{M_2} \right) \cdot \left(\frac{1}{6\pi\sqrt{3}} \right) \quad (4.21)$$

$$R = 0.375 \cdot \left(\frac{\pi}{M_4} \right)^{0.5} \quad (4.22)$$

The Gaussian distribution for the asperity heights is given as follows:

$$\Phi = \frac{(2\pi)^{-1/2}}{\sigma_s} \exp \left[-0.5 \left(\frac{z}{\sigma_s} \right)^2 \right]. \quad (4.23)$$

McCool [26] defines σ_s to be the standard deviation of the asperity heights. This is calculated from the standard deviation of the entire surface (RMS roughness):

$$\sigma^2 = \sigma_s^2 + \frac{3.717 \times 10^{-4}}{\eta^2 R^2} \quad (4.24)$$

For the GW case, the area and load are calculated using an integral of Φ and a function relating the z value to a value d . d is defined as the value above which the asperities will be in contact with the rigid flat. The compression distance, $z-d$, is the interference of the rigid flat with the asperity peaks and is known as ω for the remainder of this work. The integrals used to find the contact area, A , and the contact pressure or load, P , for each d value are given below:

$$A(d) = A_n \eta \int_d^{\infty} \bar{A}(\omega) \cdot \Phi(z) \cdot dz \quad (4.25)$$

$$P(d) = A_n \eta \int_d^{\infty} \bar{P}(\omega) \cdot \Phi(z) \cdot dz \quad (4.26)$$

For the perfectly elastic case, \bar{A} and \bar{P} are acquired from the Hertz solutions given as:

$$\bar{A}_E = \pi R \omega \quad (4.27)$$

$$\bar{P}_E = \frac{4}{3} E' \sqrt{R} (\omega)^{3/2} \quad (4.28)$$

Furthermore, surface separation can be obtained by relating the distance from the mean surface height to the rigid flat, δ , to d .

$$\delta = d + y_s \quad (4.29)$$

The value y_s is defined by Front [27] as follows:

$$y_s = \frac{0.045944}{\eta R} \quad (4.30)$$

4.5 Statistical Elastic-Plastic Contact

Similar to the multiscale model, some of the asperities will undergo plastic deformation as loads increase past the critical values. This work uses the methodology of Jackson and Green [28] and [3], referred to as JG for the remainder, which replaces the Hertzian contact solution in the GW model with equations suited for elastic-plastic deformation after critical values have been reached. The statistical method calculates load and area as a function of separation instead of area as a function of load as seen in the multiscale methods. Therefore, instead of using the critical force to define the elastic-plastic regime of contact, the critical interference is used. The critical interference value is given by [28] as follows:

$$\omega_c = \left(\frac{\pi \cdot C \cdot S_y}{2E'} \right)^2 \cdot R \quad (4.31)$$

For interference $\omega < 1.9\omega_c$, spherical contact is considered to effectively agree with the perfectly elastic Hertzian contact model. However, when $\omega \geq 1.9\omega_c$ the following equations from JG are used in place of Eqs. (4.27-4.28). This substitution will provide the necessary values to calculate the elastic-plastic behavior of the asperities in contact.

$$\bar{A}_{JG} = \pi R \omega \left(\frac{\omega}{\omega_c} \right)^B \quad (4.32)$$

$$\bar{P}_{JG} = P_c \left\{ \left[\exp \left(-\frac{1}{4} \left(\frac{\omega}{\omega_c} \right)^{5/12} \right) \right] \left(\frac{\omega}{\omega_c} \right)^{3/2} + \frac{4H_G}{CS_y} \left[1 - \exp \left(-\frac{1}{25} \left(\frac{\omega}{\omega_c} \right)^{5/9} \right) \right] \right\} \frac{\omega}{\omega_c} \quad (4.33)$$

where

$$P_c = \frac{4}{3} \left(\frac{R}{E'} \right)^2 \left(\frac{C}{2} \pi S_y \right)^3 \quad (4.34)$$

$$B = 0.14 \exp(23e_y) \quad (4.35)$$

$$e_y = \frac{S_y}{E'} \quad (4.36)$$

$$\frac{H_G}{S_y} = 2.84 - 0.92 \left(1 - \cos \left(\pi \frac{a}{R} \right) \right) \quad (4.37)$$

$$\frac{a}{R} = \sqrt{\frac{\omega}{R} \left(\frac{\omega}{1.9 \cdot \omega_c} \right)} \quad (4.38)$$

These equations are then used in Eqs. (4.25-4.26) for the single asperity area and load.

4.6 Contact Resistance

One of the concerns of this work is calculating the effect of surface roughness on electrical resistance. Therefore, the goal of this section is to determine how the flow of the current between surfaces is affected by the true area of contact for each load level. Since only a few, scattered asperities are actually in contact for any given load level, the current is restricted to very small contact patches when compared to the area of the entire surface. As the current flows through these asperity peaks, it will be effectively “bottlenecked” resulting in some resistance to the conduction as seen in Fig. 4.3 on page 23.

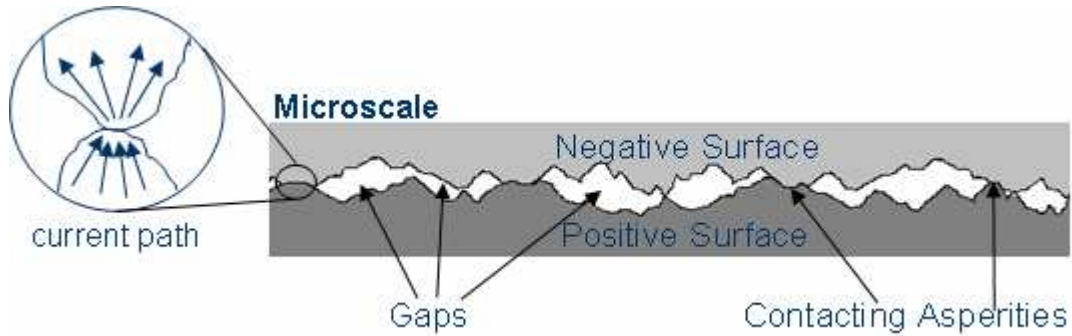


Figure 4.3: Schematic of “bottlenecked” current flow through asperities.

Holm [29] gives a simple formula to calculate the electrical resistance due to asperity contact.

$$Er_{asp} = \frac{\rho_{L1} + \rho_{L2}}{4a} \quad (4.39)$$

Where Er refers to the contact resistance value, a is the radius of contact, and ρ is the specific electrical resistance, or resistivity, of the respective surfaces. However, this equation is only good for a single asperity. In the case of both multiscale and statistical techniques, additional equations are required to calculate resistance for the entire surface, (see the following sections).

4.6.1 Multiscale Electrical Contact Resistance

The multiscale sinusoidal method presented here is an iterative method that calculates area and resistance for each particular frequency level. To predict electrical contact resistance, the first step is to calculate the average radius of contact per frequency level i :

$$a_i = \sqrt{\frac{A_i}{2 \cdot \pi \cdot A_{i-1} \cdot f^2}} \quad (4.40)$$

Once the average contact radius is established, Eq. (4.39) is implemented to calculate resistance per asperity per level. For the sinusoidal case, it is assumed that the tip of the asperity is similar to a hemisphere so the radius of curvature at the tip is used. Oftentimes, an alleviation factor is used in thermal contact resistance calculations to account for the affect of a large contact radius, a , in relation to the asperity tip radius, R . Since electrical and thermal contact resistances are very mathematically similar, it stands to reason that the alleviation factor, Ψ , should also be included for electrical contact resistance. Though there are various ways to calculate this factor [30], the simplified version offered by Cooper et al. [31] is chosen for this work:

$$\Psi_i = \left(1 - \sqrt{\frac{A_i}{A_{i-1}}} \right)^{1.5} \quad (4.41)$$

The alleviation factor, Ψ_i , is combined with the resistance value and the result is summed over all possible iteration levels to find the total resistance for the entire surface in contact. In equation form this is given as:

$$Er_{total} = \sum_{i=1}^{i_{max}} \Psi_i Er_i \eta_i A_{i-1} \quad (4.42)$$

It is important to note that this technique calculates the resistance for each frequency level and then sums them over all frequency levels to calculate the total. Another technique exists that only evaluates the resistance for the highest frequency level that still reduces contact area [32]. This alternative technique is not considered in this work. Also, this methodology does not change depending on the inclusion of plasticity since all resistance calculations are done after obtaining the contacting area.

4.6.2 Statistical Electrical Contact Resistance

To continue comparing the multiscale results with that of the earlier statistical method (see section 4.4 and 4.5), the electrical contact resistance is also obtained for statistical perfectly elastic and elastic-plastic methods. Greenwood and Williamson [1] include a solution for contact conductance in their work. Resistance is simply the inverse of conductance so the technique for calculating perfectly-elastic contact resistance is as follows:

$$\frac{1}{Er_e(d)} = 2A_n \eta \Psi \rho_L^{-1} R^{1/2} \int_d^\infty \omega^{1/2} \cdot \Phi(z) \cdot dz \quad (4.43)$$

Note the inclusion of the alleviation factor, Ψ . The statistical method is not a multiscale procedure so the alleviation factor is calculated as follows:

$$\Psi = \left(1 - \sqrt{A_r/A_n}\right)^{1.5} \quad (4.44)$$

Contact resistance from elastic-plastic statistical contact is calculated in the same manner except using a different elastic-plastic asperity contact model. One such technique is given by Kogut and Etsion [33], which is used as an outline for this work. However, there are dissimilarities since this work relies on the methodology of Jackson and Green [28] for single asperity contact. Eq. (4.43) is still used but the contact radius, a , has changed in accordance with the work of Jackson and Green:

$$a_{ep} = \sqrt{D\omega R} \quad (4.45)$$

where if $0 \leq \omega/\omega_c \leq 1.9$, then $D = 1$, but if $\omega \geq 1.9\omega_c$, then $D = \left(\frac{\omega}{1.9\omega_c}\right)^B$.

By applying the contact radius in Eq. (4.45) to the resistance calculation in Eq. (4.43), the elastic-plastic electrical contact resistance is obtained.

$$\frac{1}{Er_{ep}(d)} = A_n \eta \Psi \int_d^{\infty} \frac{2a_{ep}}{\rho_L} \cdot \Phi(z) \cdot dz \quad (4.46)$$

Similar to the multiscale model, the alleviation factor, ψ , is included here as well.

4.7 Thermal Contact Resistance

Thermal contact resistance refers to the build-up of heat at the boundary between the two surfaces due to the same “bottleneck” effect referred to in electrical resistance seen in Fig. 4.3 on page 23. Technically, heat can flow across the gaps in the material as well as through the contacting asperities. However, the heat transfer across the gaps is neglected since like electrical current, usually the majority of the heat flow will follow the path of least resistance or in this case the asperities in contact. Indeed, thermal and electrical contact resistances are very similar effects and are computed using very similar methods as well.

The thermal resistance values for the multiscale contact methods are found by modifying Eqs. (4.41-4.42) as follows:

$$Tr_{asp} = \frac{\rho_{T1} + \rho_{T2}}{4a} \quad (4.47)$$

$$Tr_{total} = \sum_i^{i_{max}} \Psi_i Tr_i \eta_i A_i \quad (4.48).$$

In this case, ρ_T refers to the thermal resistivity or inverse of the conductivity of the material.

Similarly, thermal contact resistance for statistical methods is obtained by substituting thermal resistivity for electrical resistivity in Eqs. (4.43-4.46).

$$\frac{1}{Tr_e(d)} = 2A_n \eta \Psi \rho_T^{-1} R^{1/2} \int_d^\infty \omega^{1/2} \cdot \Phi(z) \cdot dz \quad (4.49)$$

$$\frac{1}{Tr_{ep}(d)} = A_n \eta \Psi \int_d^\infty \frac{2a_{ep}}{\rho_T} \cdot \Phi(z) \cdot dz \quad (4.50)$$

4.8 Scale Dependent Thermal Contact Resistance

Scale dependency is an emerging topic in the field of contact resistance. The concept behind scale dependency is that as a sample of a material is viewed at increasingly higher magnification the material properties actually change according to how small of a sample is viewed. The reason for this is that at some point one is viewing actual atoms pressed against each other instead of the continuous material. Therefore, at this point the scale is below that where most imperfections and features are seen, such as grain boundaries. This impacts the multiscale contact model because it takes into account many different scales of asperities down to where this phenomenon is seen. To include these effects, the thermal contact resistance, Eqs. (4.47-4.50), is replaced with a scale dependent value found in the work of Prasher and Phelan [34]:

$$Tr_{SD} = \frac{\Psi}{2ka} \left(1 + \frac{8}{3\pi} Kn \right) \quad (4.51)$$

Kn refers to the Knudsen number $\left(\frac{\lambda_{MFP}}{a} \right)$ where λ_{MFP} is the phonon mean free path.

$$\lambda_{MFP} = \frac{3k}{\rho v_s C_p} \quad (4.52)$$

Here, ρ is the density of the material, v_s refers to the solid speed of sound, C_p is the heat capacity, and k is the thermal conductivity. Note also that the alleviation factor, Ψ , has been included in the scale-dependent calculations although it is not part of the Prasher and Phelan [34] solution.

4.9 Convergence of Real Area of Contact

As mentioned previously, the data set used for this model is converted into a series of stacked sine waves using the discrete Fourier Transform. All calculations for the model are then made based off the amplitude and wavelength of these sine waves. The multiscale model considered here assumes that the predicted area converges as all scales are included in the model. This is important because if the predictions do not converge then the area will approach zero as smaller scales are included, as was predicted by [35]. In order to test convergence, a power fit is found for the nominal amplitude as a function of wavelength.

$$\Delta_i = \alpha \lambda_i^\gamma \quad (4.53)$$

where λ_i is the wavelength (inverse of frequency) and both α and γ are constants derived by fitting Eq. (4.17) to the Fourier series of the surface data. For a particular surface the best fit was found with $\alpha=.085$ and $\gamma=1.5$. Starting with this “benchmark case”, the values α and γ are then varied individually to find any critical values at which point convergence is not possible. This process is carried out for both perfectly elastic and elastic plastic cases. The results are provided in Chapter 6.2

4.10 Adjusted Statistical Surface Separation

Through comparison to the sinusoidal multiscale technique, a potential error is brought to light in the statistical methods. When calculating surface separation, the statistical models show a significant surface separation despite the calculated real area of contact reaching its maximum value. This result is highly unexpected since there should be no separating gap if the two surfaces are entirely in contact as seen in the multiscale modeling results. The reasons for difference amongst the statistical and multiscale methods are three-fold. First, in the multiscale method, all asperities are loaded equally so they may actually be over-compressed. Second, the statistical model does not consider the interactions between adjacent asperities. At some loads, the valleys neighboring each peak may be rising as they fill in with the plastically deformed material. Third, believed to be the most important, the statistical method does not adjust the mean height based on asperity deformation.

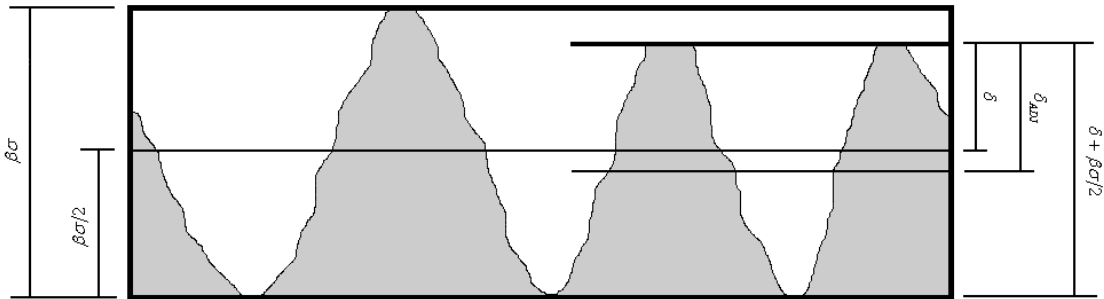


Figure 4.4: Graphical comparison of surface separation and adjusted surface separation.

To improve agreement between the models, an adjusted separation is now implemented. As shown schematically in Fig. 4.4, the adjusted separation, δ_{ADJ} , is found by assuming that the mean height when considering deformation will locate at the

midpoint between the deformed tips of the asperities and the deepest valleys of the asperities. Therefore, as the surface deforms due to contact, the mean surface height actually changes from $\beta\sigma/2$ to a smaller value. Using this concept, the surface separation predicted by the statistical model can be adjusted using the following simple equation:

$$\delta_{ADJ} = \frac{\delta + 0.5\beta\sigma}{2} \quad (4.54)$$

As seen in Fig. 4.4, Eq. (4.54) takes the average of the mean surface height at zero deformation, $\beta\sigma/2$, and the distance from the mean surface height to the peak of the deformed surface, δ . The β value is found not to be constant and varies not only for different surfaces but also depends on whether plasticity is considered. As shown in Fig. 4, $\beta\sigma$ represents the peak to valley height of the surface. Since statistically 68% of the asperities are accounted for between -2σ and 2σ and 99.7% are accounted for between -6σ and 6σ , one could make an approximation of β between 4 and 12.

CHAPTER 5

EXPERIMENTAL DESIGN

One of the many issues in the field of contact mechanics is the validation of the many different contact models. Problems arise in experimental validation because the surface features and behaviors mentioned in works of this type are often at extremely small scales. An additional dilemma is that typically metals are the material of choice for studying contact mechanics. These and other issues result in no efficient and reliable way to “view” the real area of contact to compare to theoretical results. Therefore, the experimental test apparatus for this work is designed to measure electrical contact resistance. This surface characteristic is much easier to accurately calculate and the choice of metals actually aids the process since most metals are very good conductors.

To compare with the theoretical calculations for electrical contact resistance, the testing procedure must be able to alter the load placed upon the test samples and measure the change in resistance at the interface of the test surfaces. In this case, the test is also designed to garner measurements for a variety of roughness. The samples used are all as close to identical as possible. The roughness is changed by sanding each surface with a different grit of sandpaper to altering the roughness left from machining and selecting one surface to be the common base to use against the remainder. After selecting and altering the samples, a stylus profilometer is used to measure the exact roughness and profile for

each sample. Then a copper wire is attached to each sample which will be the connection for a multi-meter set up to measure the voltage drop across the contacting surfaces.

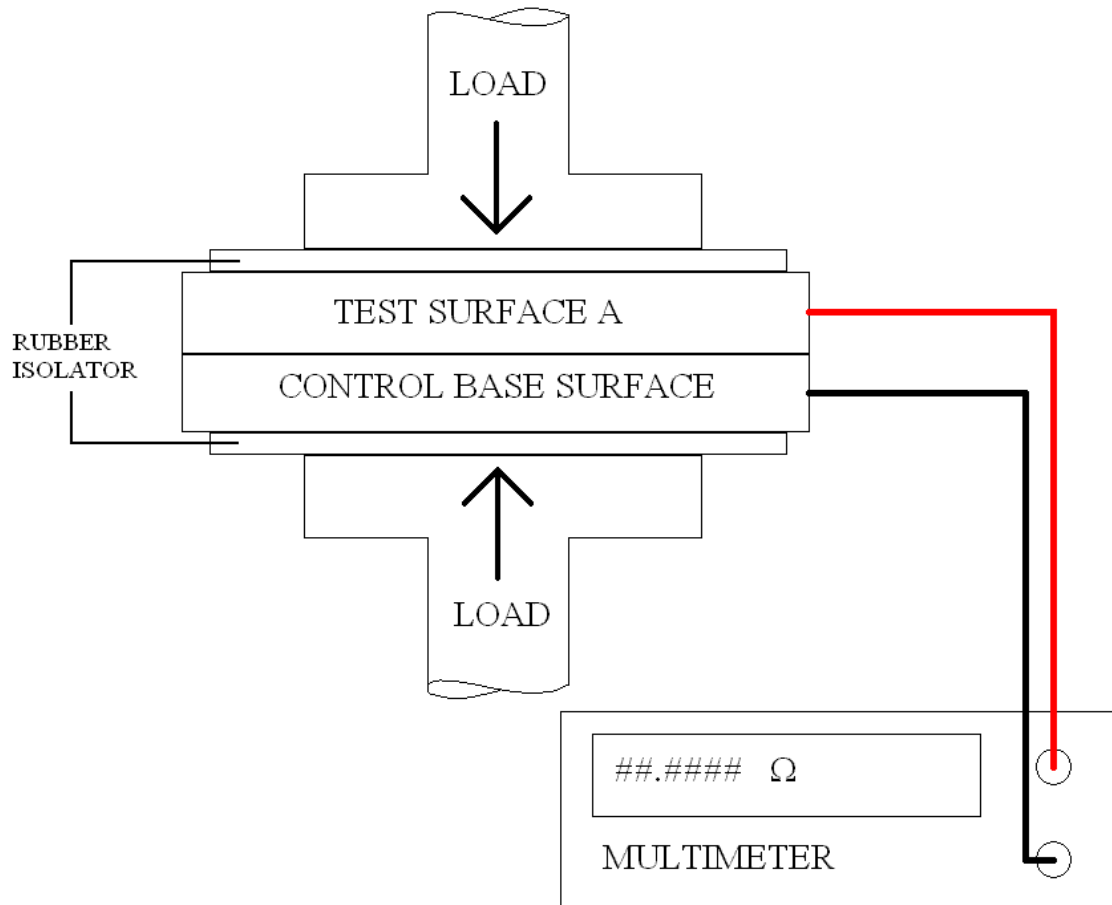


Figure 5.1: Schematic of electrical contact resistance test apparatus.

Finally, a modified drill press is used to press the two surfaces together for the desired loads as seen in Fig. 5.1. A load cell is used to ensure accurate readings through Labview™ software. In this test, weights are applied to the drill press to increase the pressure upon the two surfaces in increments. At each load increment, the multi-meter is used to calculate the electrical resistance of the samples in contact. This value is a

measure of the voltage drop across the surface due to incomplete contact and is expected to correspond to the theoretical results for the load applied.

Unfortunately, only a few initial runs were attempted with this test apparatus which proved to be unsuccessful. The results were very inconsistent in that for the first few increments of load, the resistance would indeed drop but as greater and greater loads were added the resistance would increase, sometimes to its original value. Also, the resistance values would not reach a consistent value. Instead the resistance would rise and fall within a range that furthered the inaccuracy of the results. One issue in setting up this experiment, which most likely led to the resistance issues, was the sample material available at the time of testing was a steel tab being pressed against a polished stainless steel block. Getting a consistent connection from the copper wires of the multimeter to these steel samples was very difficult since tin solder does not hold on steel. Therefore, any connection made turned out to be extremely fragile. To remedy these issues, this experiment will be attempted later using samples of different materials which should be easier to manipulate and measure.

CHAPTER 6

RESULTS

6.1 Introduction

This chapter is devoted to the calculated results from the theoretical models. The first section reveals the results of a convergence analysis for the sinusoidal multiscale model. For the second section, a single surface is used so the roughness remains constant. This is done to compare the results of the sinusoidal based multiscale model with that of the statistical technique for both perfectly elastic and elastic-plastic deformations cases with the intention of validating the new multiscale technique with the familiar statistical model. Third and final is a section that gives a direct view of the effects roughness has upon the calculated theoretical values.

6.2 Convergence of Real Contact Area

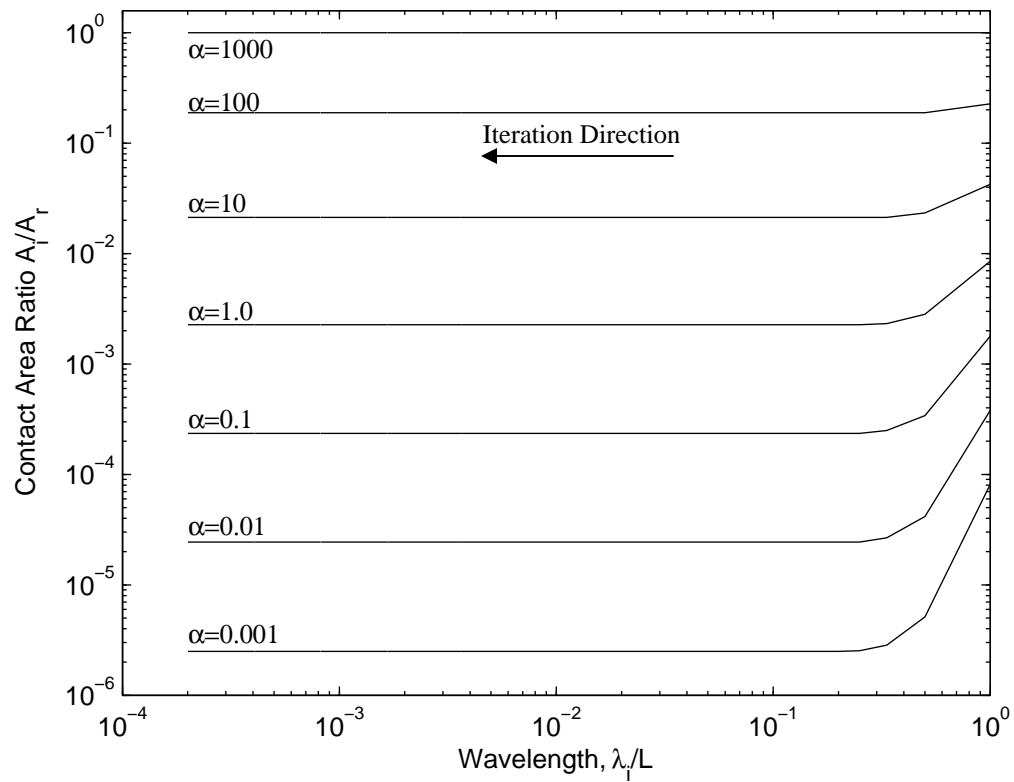


Figure 6.1: Contact area ratio as a function of wavelength for perfectly elastic multiscale method where α is varied in Eq. (4.53).

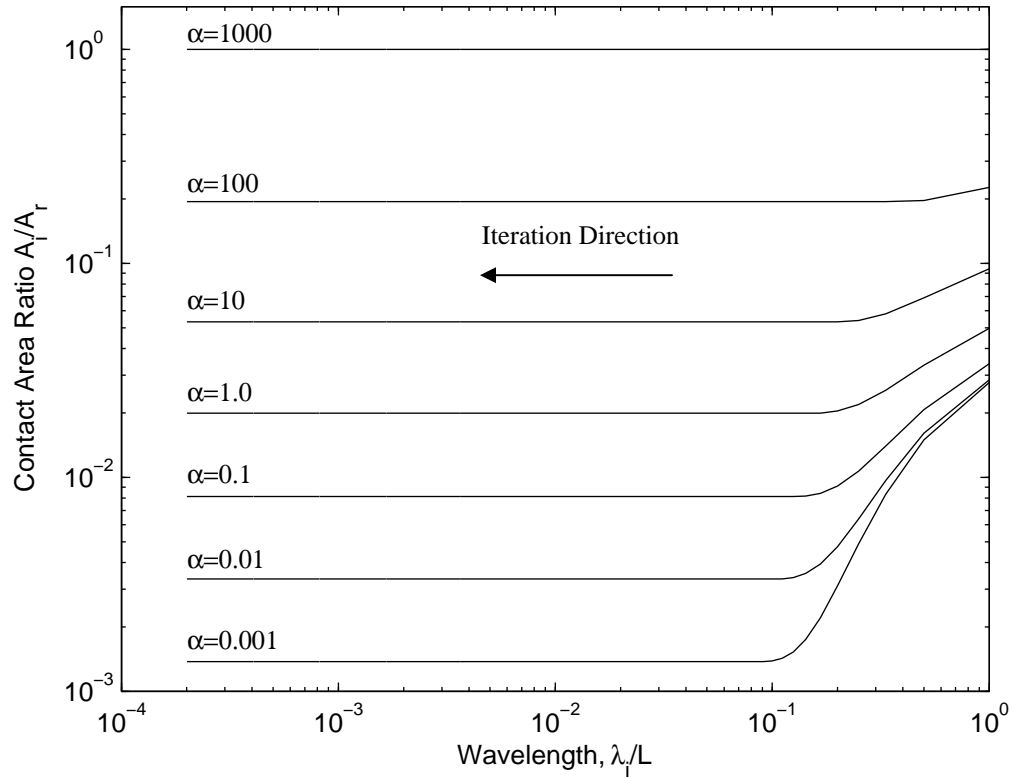


Figure 6.2: Contact area ratio as a function of wavelength for elastic-plastic multiscale method where α is varied in Eq. (4.53).

The first test of convergence is to characterize the role that α plays in Eq. (4.53). For this test case, α is varied from 10^{-3} to 10^3 by an order of magnitude at each step. The fit value for α was found to be 0.085, which falls within the range of values tested. As seen in Fig. 6.1-6.2, α does not appear to play a significant role in convergence since all the lines show a flattening trend at the smaller wavelengths. This result is independent of plasticity since nearly the same trend is seen in both Figs. 6.1-6.2.

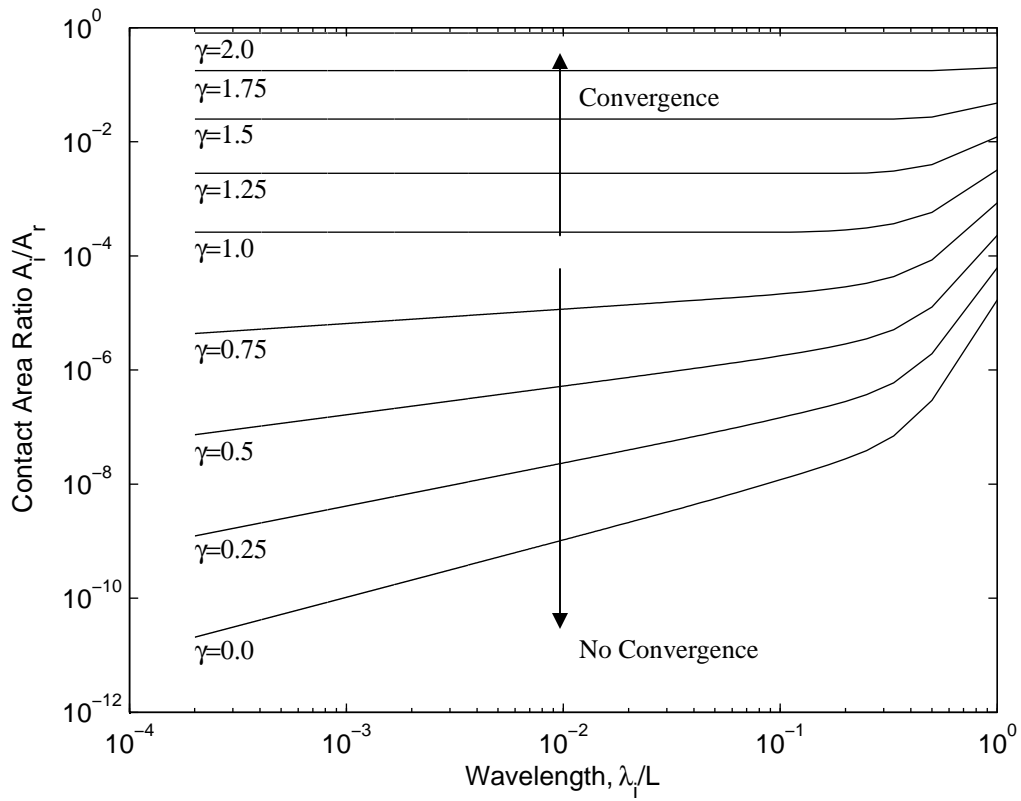


Figure 6.3: Contact area ratio as a function of wavelength for perfectly elastic multiscale method where γ is varied in Eq. (4.53).

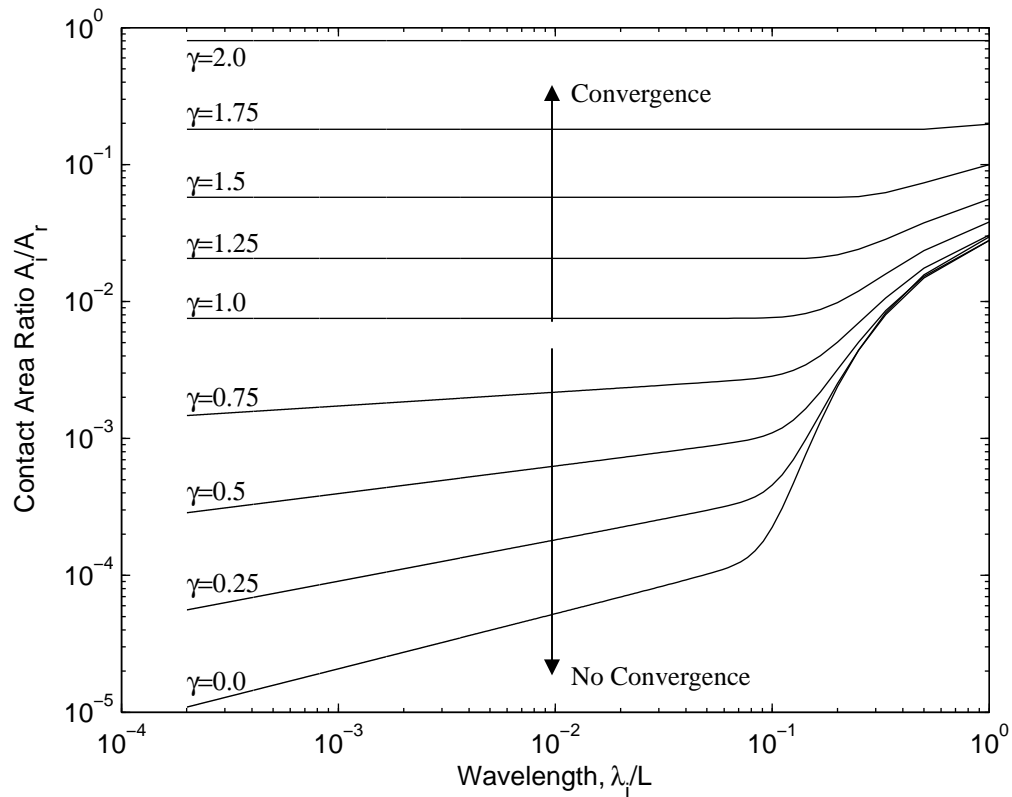


Figure 6.4: Contact area ratio as a function of wavelength for elastic-plastic multiscale method where γ is varied in Eq. (4.53).

The second test of convergence is conducted by varying the value of γ in Eq. (4.53). The results from this test, shown in Figs. 6.3-6.4, show that this exponent is the deciding factor for convergence in both perfectly elastic and elastic-plastic cases. For this test γ is varied from 0 to 2 at intervals of 0.25. For a good fit to the FFT data, γ was found to be 1.5, which is within the range of values tested. γ values lower than 1 show a continual slope despite the wavelength size suggesting that convergence is not possible for these cases. This result is shown to be similar for both perfectly elastic and elastic-plastic cases.

The results of these tests have shown that convergence is dependent upon the exponent, γ , in the power function fit to the FFT data in Eq. (4.53). As the scales are iteratively included, the contact area reduces. Therefore, the average pressure continues to increase and may eventually become larger than the pressure to cause complete contact (p^*). If this pressure stays above the pressure to cause complete contact (p^*) the area will no longer reduce and convergence is obtained. Therefore, for convergence to occur, p^* must stay constant or decrease as λ decreases. This suggests that the requirement for convergence depends upon the following relationship:

$$p^* \propto \frac{\Delta}{\lambda} = \alpha \lambda^{\gamma-1} \quad (4.55)$$

As long as Δ/λ stays constant or decreases as λ decreases then the multiscale sinusoidal method will converge. This condition is met as long as the γ value in Eqs. (4.53 & 4.55) are greater than or equal to 1, as shown by Eq. (4.55).

$S_y = 14 * 10^6 Pa$	$E = 41.369 * 10^9 Pa$
$\rho_L = 11.5 * 10^{-8} \Omega \cdot m$	$\nu = 0.36$

Table 6.1: Material Properties of Tin

6.3 Contact Resistance Model Comparison

This part of the work assumes realistic material properties for all results gathered (see Table 1). Since this work includes an examination of electrical resistance, the material of choice is Tin due to its common use in electrical connectors and circuits. The surface profile is measured from machined metal samples using a stylus profilometer. To ensure an accurate comparison of the contact models, the material properties and surface

geometry are kept constant for all calculations. For actual calculations, Matlab™ is used for evaluating mathematical results.

Once the data is gathered, a Fast Fourier Transform is performed as mentioned before. The result is then converted to amplitude via the complex conjugate. Then multiscale models can be calculated as described above. For the GW and JG models, the statistical parameters are acquired using McCool's [26] methods by finding the spectral moments about the surface (see Appendix II). From here, the GW model is fairly straightforward except for the integrals. To solve these, numerical integration techniques are employed. Simpson's Method is used by first breaking the integral into 1000 sub-intervals and performing the Simpson's interpolation on each subinterval.

6.3.1 Calculated Real Area of Contact

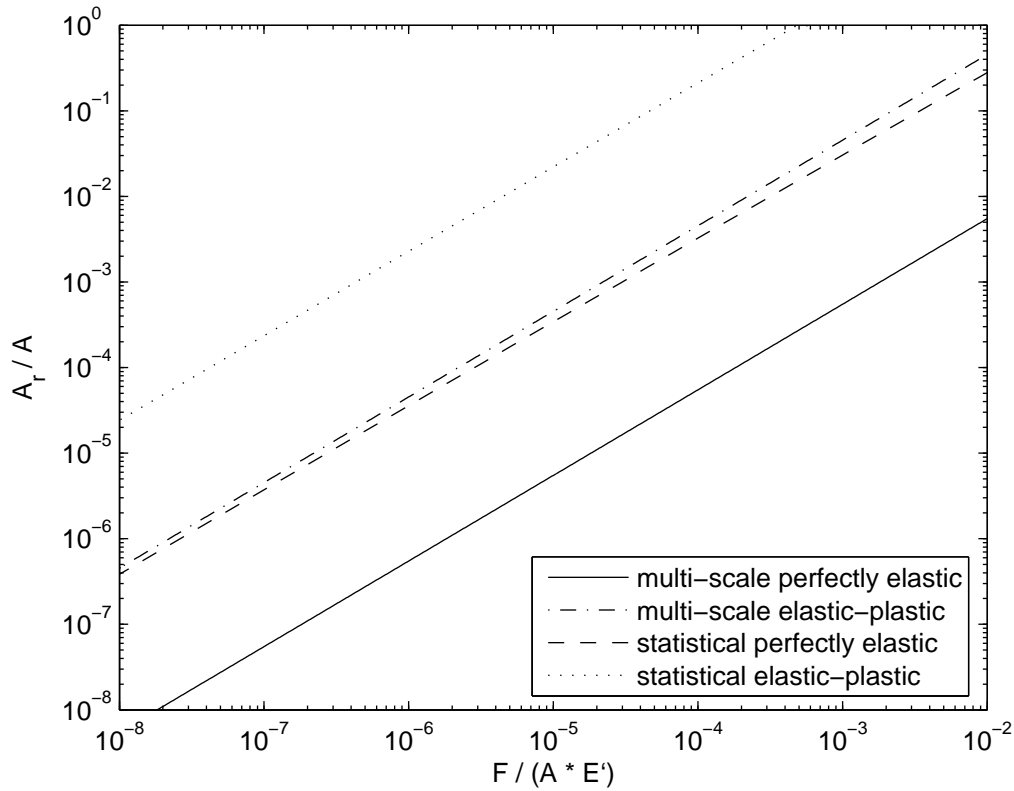


Figure 6.5: Non-dimensional area vs. load.

As seen in Fig. 6.5, higher loads result in a greater area of contact for the two surfaces. The comparison of the two modeling techniques resulted in good qualitative agreement but poor quantitative agreement. Greater contact area also results from the inclusion of plastic deformation. This is caused by the behavior of the solid asperities to flow and flatten when plastic deformation is included. The asperity material tends to “flow” resulting in greater deformation as well as “filling in” the low spots around each asperity. This combines with the higher loads to produce larger amounts of contact. These two techniques are calculated in very different manners using almost no common

equations. However, all the methods displayed here show the linear relation between real contact area and load. Therefore, this qualitative agreement serves to confirm the accuracy of the trends of both methods for modeling the contact of rough surfaces.

6.3.2 Surface Separation

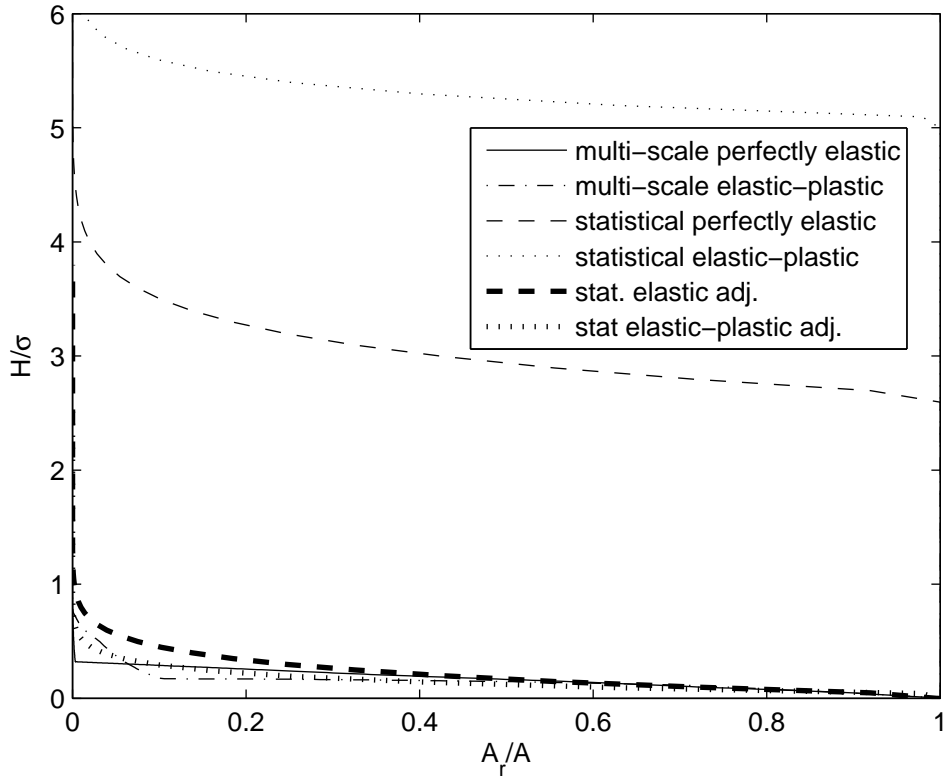


Figure 6.6: Area compared to Surface Separation including the adjusted separation for Statistical Contact Methods.

The surface separation as a function of the calculated real area of contact is shown in Fig. 6.4. Although the overall trends of the two models are similar, the calculations for the statistical methods both show the surfaces in full contact before the surface separation

has reached zero. Logically, when contact is complete, the real area of contact should be at its maximum and surface separation should be zero. To alleviate this possible error, Eq. (4.54) is used in the adjusted results seen above (bold lines in Figs. 6.6 and 6.7). For the surface data considered in the current analysis a value of $\beta=5.2$ was found to work well for the perfectly elastic case. However, for elastic-plastic deformation, $\beta=10.02$ produced the appropriate results. These adjustments will be different for each case because the amount of compression and deformation will be different for the perfectly elastic and elastic-plastic cases. The resulting adjusted statistical model results are shown in Fig. 6.6.

As expected, greater loads as well as plastic deformation serve to decrease the gap between the surfaces as shown in Fig. 6.7. This is logically correct since greater loads increase the area of contact through deforming the asperities. One would expect the flattening of the asperities to allow the surfaces to come closer to each other and eventually contact completely when the calculated area is equal to the nominal area. The adjustment given by Eq. (4.54) once again improves the agreement between the statistical and multiscale methods.

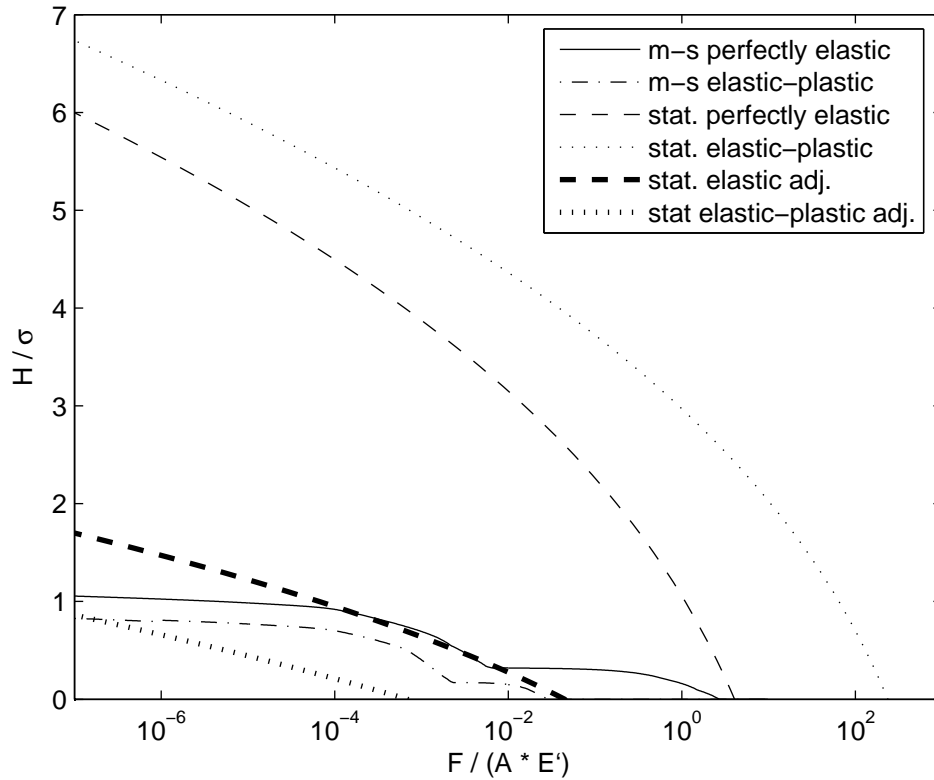


Figure 6.7: Non-dimensional surface separation vs. load.

Perhaps surprisingly, the models predict similar results on the same order of magnitude. Once again the overall trends of both the statistical and multiscale methods are confirmed by one another. In this case though, the estimated behavior of the separation is fairly different. Both methods show the decreasing gap with greater loads but they follow significantly different curves.

Without strong experimental confirmation, it is difficult to ascertain the accuracy of either model. However, the current multiscale model will result in larger contact stiffness than predicted by the statistical models. Stiffness is defined as the change in

contact force per change in surface separation. This appears to agree with experimental findings by Drinkwater et. al. [36] using acoustic methods.

6.3.3 Electrical Contact Resistance

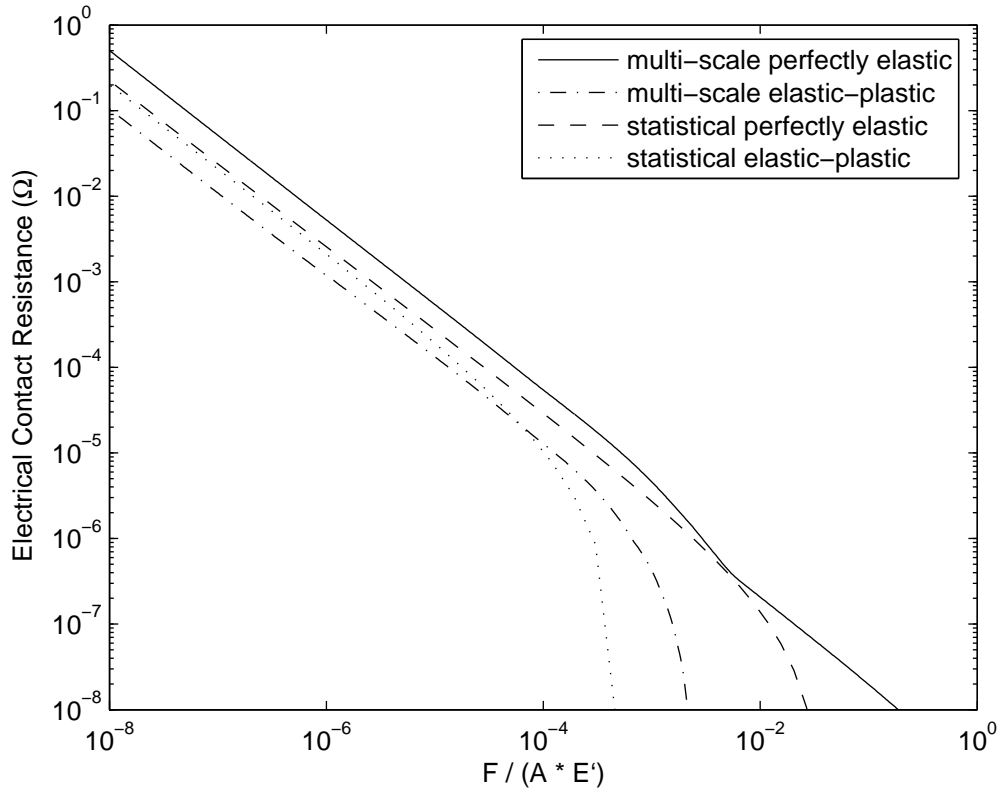


Figure 6.8: Electrical contact resistance as a function of non-dimensional load.

For the particular case of modeling the contact of an electrical connector, one concern was the amount of electrical resistance due to the “bottleneck” effect of contacting asperities. Fig. 6.8 shows the calculated results for this effect and compares the results for the multiscale and statistical models described in Chapter 4. Since the electrical resistance is due to the gaps between the surfaces, it follows naturally that the

electrical resistance decreases with load which as expected is inverse to the behavior of contact area. Yet again, when compared to the perfectly elastic cases, the elastic plastic cases require a lower load for all resistance values which implies a greater contact area at each load. The multiscale and statistical models also agree surprisingly well even though they make different predictions for contact area. This suggests that it can be difficult to validate these models based on contact resistance measurements alone. Interestingly, the ECR appears to decrease rapidly as complete contact is approached (as seen by the elbows at the end of each curve).

6.3.4 Thermal Contact Resistance

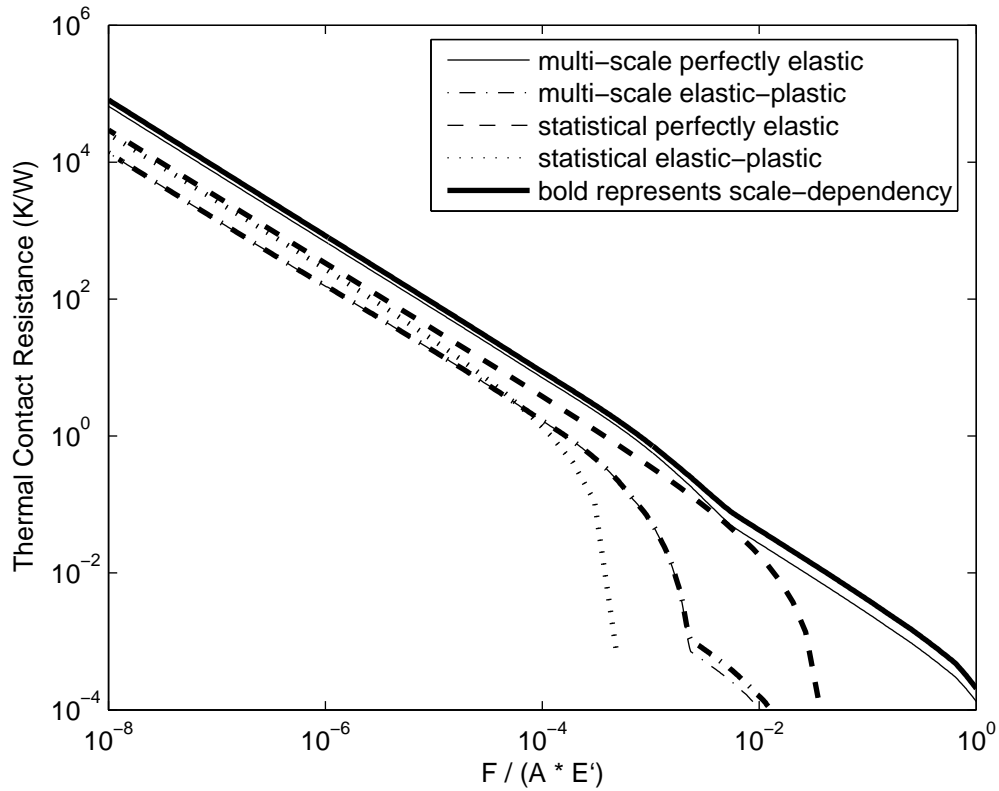


Figure 6.9: Thermal contact resistance as a function of non-dimensional load including scale-dependent results.

Thermal contact resistance is very similar to ECR because it is a measure of resistance to heat flow due to a reduced area of contact. Figure 6.9 displays the model results concerning thermal contact resistance. As can be seen, higher loads result in lower resistance values. This is due to the increased amount of material in contact thus reducing the impedance to heat flow. The values depicted are extremely similar to that of electrical resistance and this is to be expected given that they are calculated in similar manners and the flow of heat and flow of electricity are mathematically equivalent.

The bold lines shown represent the scale-dependent thermal contact resistance (see Eq. (4.51)). Scale dependency results in only slightly higher resistance values and in some cases does not appear to have any affect at all. Note that in the cases where scale dependency has no effect, the bold line in Fig. 6.9 is overlapping the non-scale dependent line preventing it from being seen. The current work finds that the inclusion of scale dependant single asperity thermal contact resistance does not affect the predicted overall thermal contact resistance significantly for the sinusoidal based multiscale rough surface contact model. This is also confirmed for the different spherical based multiscale contact model by Jackson, Bhavnani, and Ferguson [32].

6.4 Comparison between Multiple Surfaces

The next concern is what effect real multiscale roughness plays in the contact area, separation, and resistance for different surfaces. To measure this effect, multiple surface profiles were obtained using a stylus profilometer on four surfaces with roughness varying from 0.24 μm up to 5.82 μm . Fig. 6.10 shows that the smoother profiles are relatively flat where the roughest shows rather large changes in surface heights.

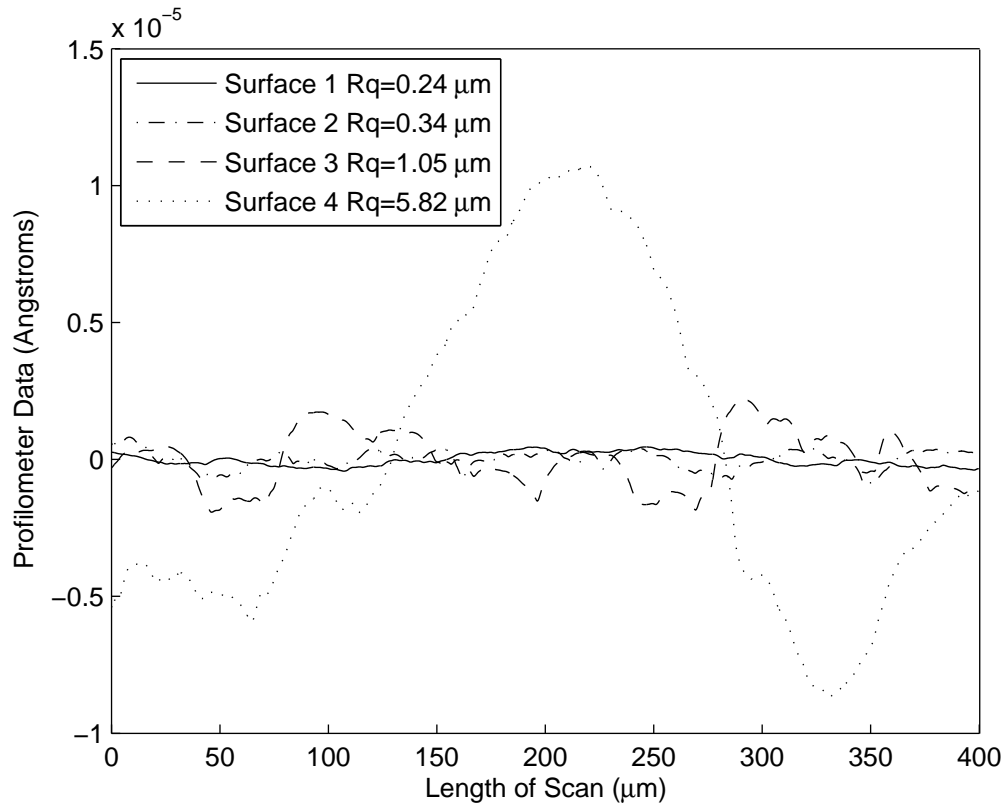


Figure 6.10: Surface profile data with different roughness values.

Surface	Roughness	α in Eq. 4.53	γ in Eq. 4.53	RMS Error of FFT to Fit
1	0.24 μm	0.13	1.60	0.3322
2	0.34 μm	0.085	1.5	0.4134
3	1.05 μm	.037	1.4	0.4053
4	5.82 μm	.006	1.0	0.0678

Table 6.2: Rough Surface Characteristics and Convergence Variables.

Table 6.2 provides a comparison between roughness and the coefficients of the power equation, Eq. (4.53), fit to the Fourier transform for each of the four surfaces

examined in this work. The root-mean-square error between the fit and FFT data is given as well. Some of the error values are quite high due to the scattering of the FFT data which does not allow for a precise fit. In application, this could result in large differences in the model predictions when a power equation is used versus the actual data. In the current work the actual data is used in the multiscale model. It is important to note that the values for α vary seemingly independent of roughness whereas γ behaves inversely of roughness. Therefore, the roughest surface has $\gamma=1.0$ which is at the limit of convergence as seen in Figs. 6.3-6.4. Therefore there may be some very rough surfaces for which the multiscale technique will not converge. This is not a concern for relatively smooth surfaces however.

6.4.1 Calculated Real Area of Contact

The following section describes the effects of surface roughness on each of the four modeling techniques, sinusoidal based multiscale elastic-plastic and perfectly elastic as well as the statistical elastic-plastic (JG) and perfectly elastic (GW). Each model is compared for four surfaces of greatly varying roughness. The values of the roughness can be seen above in Table 6.2. In this case, all results are non-dimensional. The y-axis features the calculated real area of contact divided by the apparent or nominal area of contact. The nominal area is the maximum possible area that can come into contact. The x-axis is the range of normalized loads over which the calculations are made. The load is normalized by dividing by nominal area of contact and the elastic modulus (E').

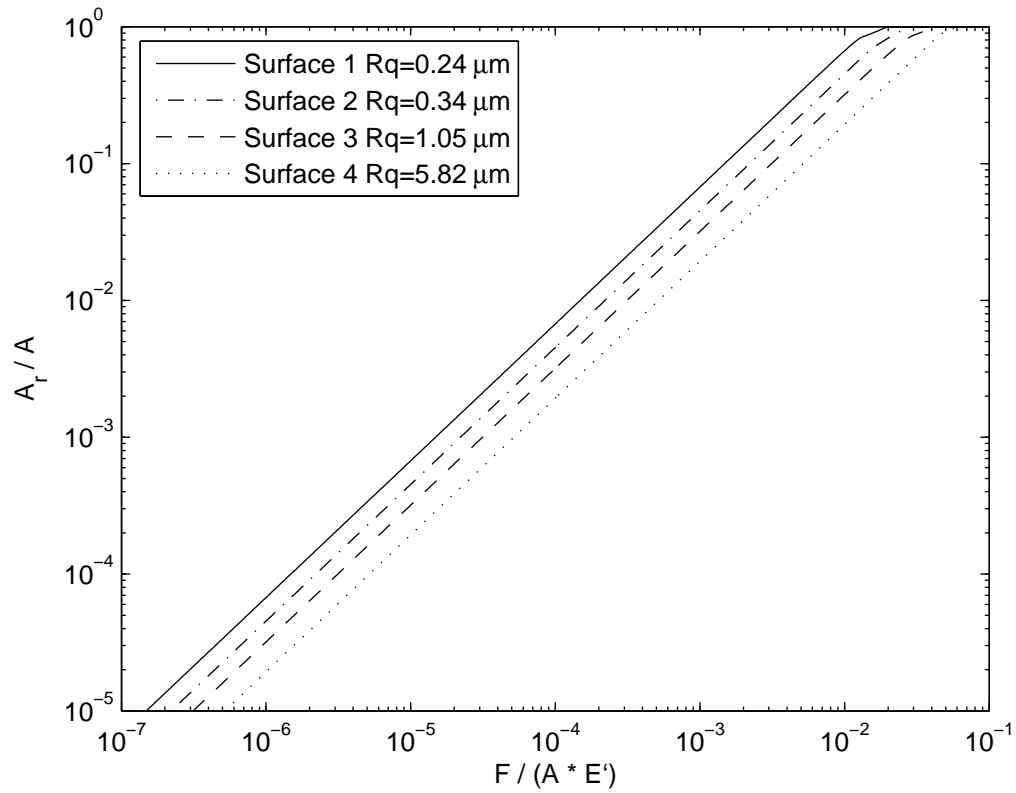


Figure 6.11: Real area of contact as a function of dimensionless load for surfaces of different roughness modeled using the sinusoidal based multiscale method for elastic-plastic material deformation.

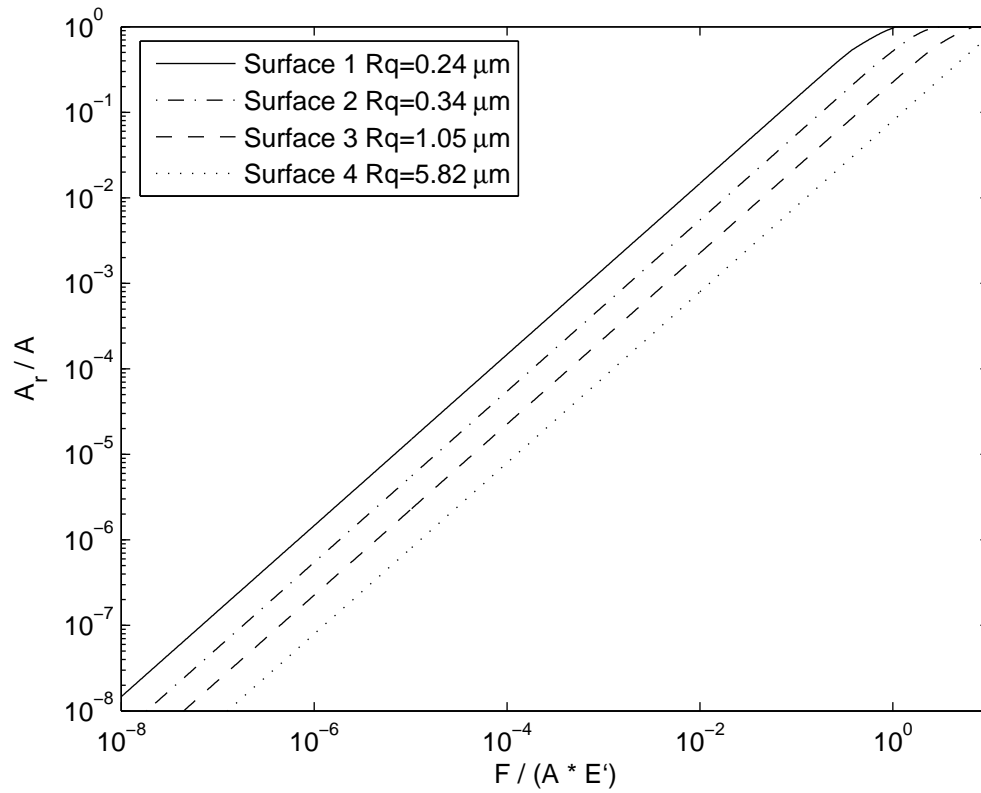


Figure 6.12: Real area of contact as a function of dimensionless load for surfaces of different roughness modeled using the sinusoidal based multiscale method for perfectly elastic material deformation.

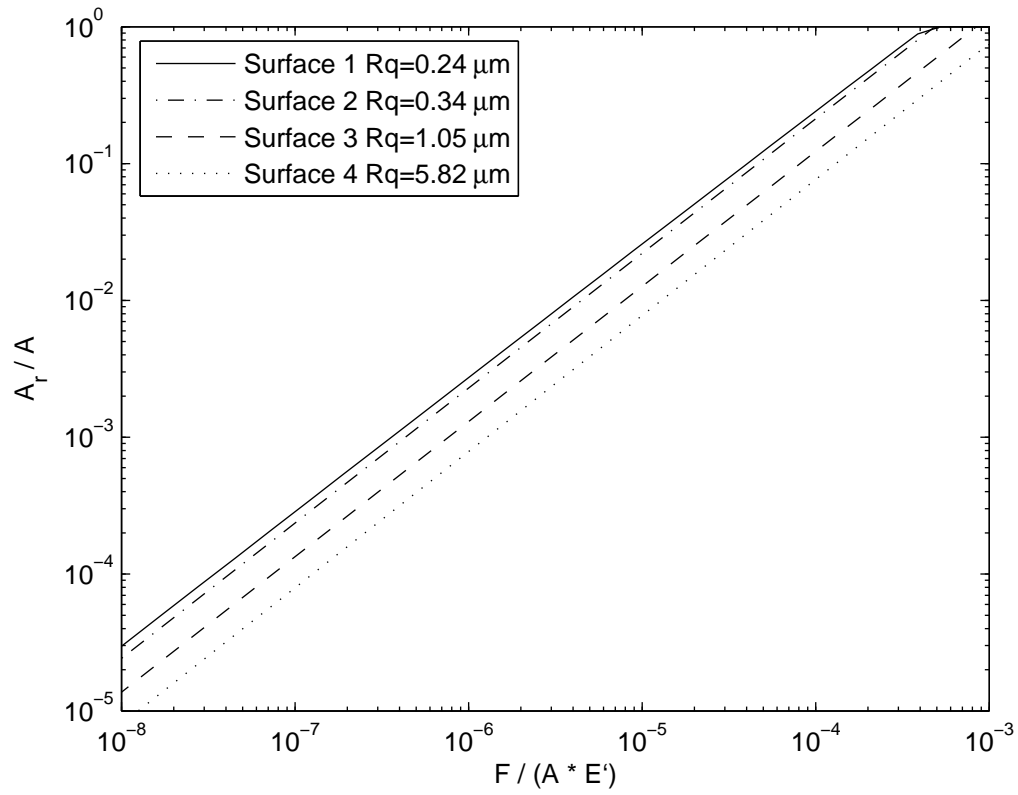


Figure 6.13: Real area of contact as a function of dimensionless load for surfaces of different roughness modeled using the JG statistical method for elastic-plastic material deformation.

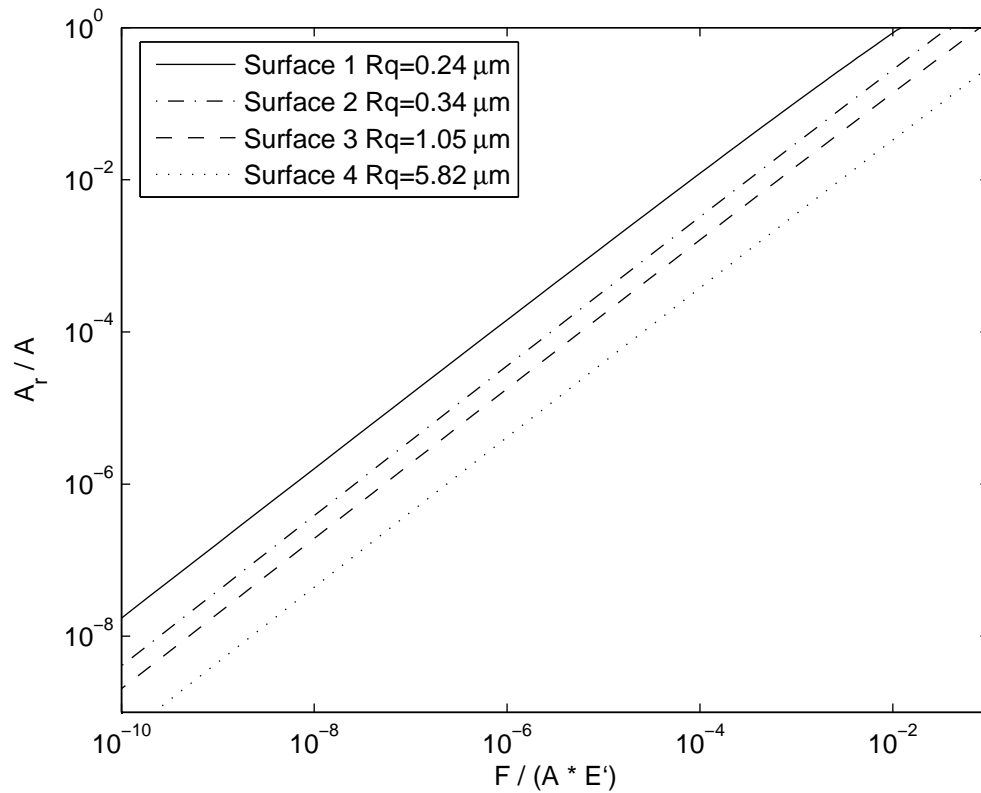


Figure 6.14: Real area of contact as a function of dimensionless load for surfaces of different roughness modeled using the GW statistical method for perfectly elastic material deformation.

As seen in Fig. 6.11-6.14, the real area of contact changes, but remains in the same orders of magnitude despite the different roughness values of the four profiles. This results in the predicted real area of contact being extremely similar despite the change in roughness between surfaces. However, as is expected, the graph does show that the results are ranked in order of decreasing roughness with smoother surfaces showing a greater contact area for each load level. It is interesting to note that the inclusion of plasticity (Figs. 6.11 & 6.13) do not show as great a separation between each surface as

the perfectly elastic models (Figs. 6.12 & 6.14). Also, the models vary when viewing what force is required to reach full contact ($A_r/A=1$) although, in general, the elastic-plastic models require less force to reach full contact than the perfectly elastic models for either sinusoidal based multiscale or statistical techniques.

6.4.2 Surface Separation

The results seen in this section show the effects of surface roughness on surface separation. As described previously, this is the difference between the mean heights of the two surfaces as they are pressed together. The first four graphs, Figs. 6.15-6.18, give results for surface separation as compared to non-dimensional load. For these four the units of the y-axis are for dimensionless surface separation by dividing the calculated separation with the standard deviation, σ . The remaining graphs of this section, Figs. 6.19-6.22, display the same dimensionless surface separation but as a function of dimensionless area (A_r/A). It is important to note that the statistical modeling results (Figs. 6.17, 6.18, 6.21, & 6.22) are all calculated using the adjusted method suggested by Eq. (4.54).

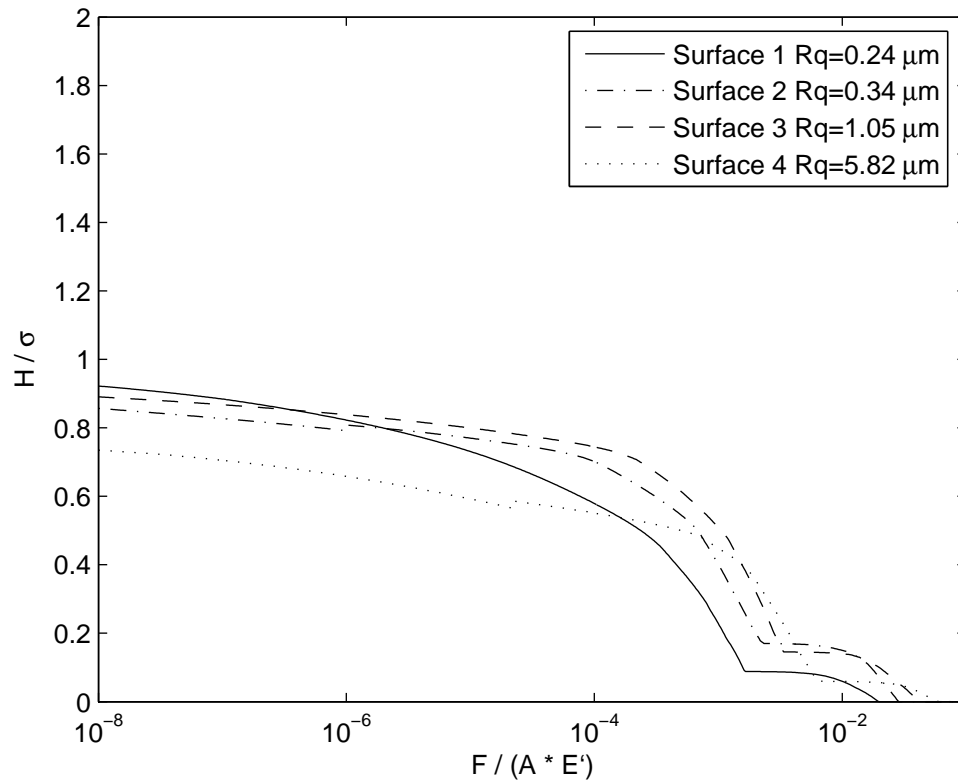


Figure 6.15: Surface Separation as a function of dimensionless load for surfaces of different roughness modeled using the sinusoidal based multiscale method for elastic-plastic material deformation.

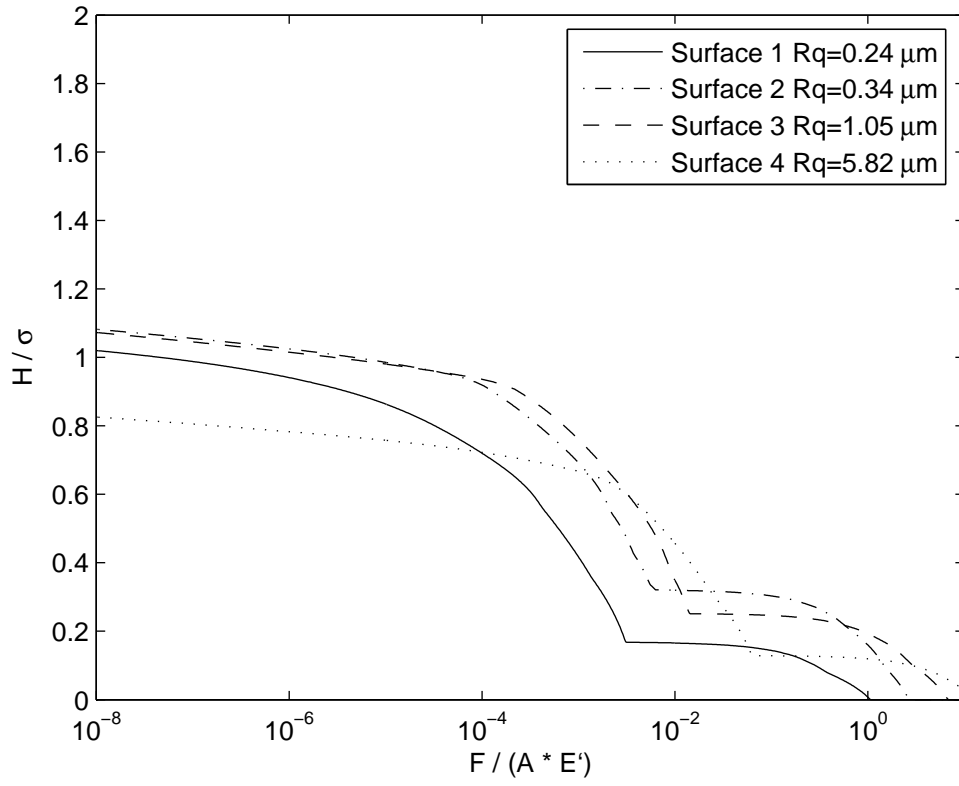


Figure 6.16: Surface Separation as a function of dimensionless load for surfaces of different roughness modeled using the sinusoidal based multiscale method for perfectly elastic material deformation.

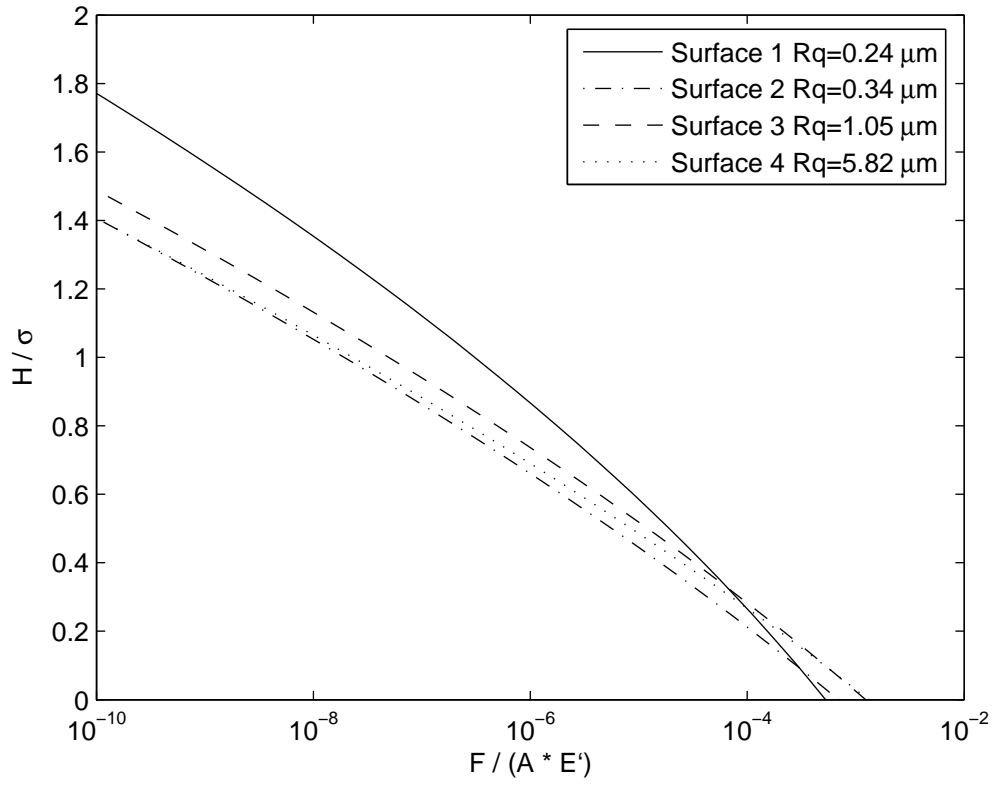


Figure 6.17: Surface Separation as a function of dimensionless load for surfaces of different roughness modeled using the JG statistical method for elastic-plastic material deformation.

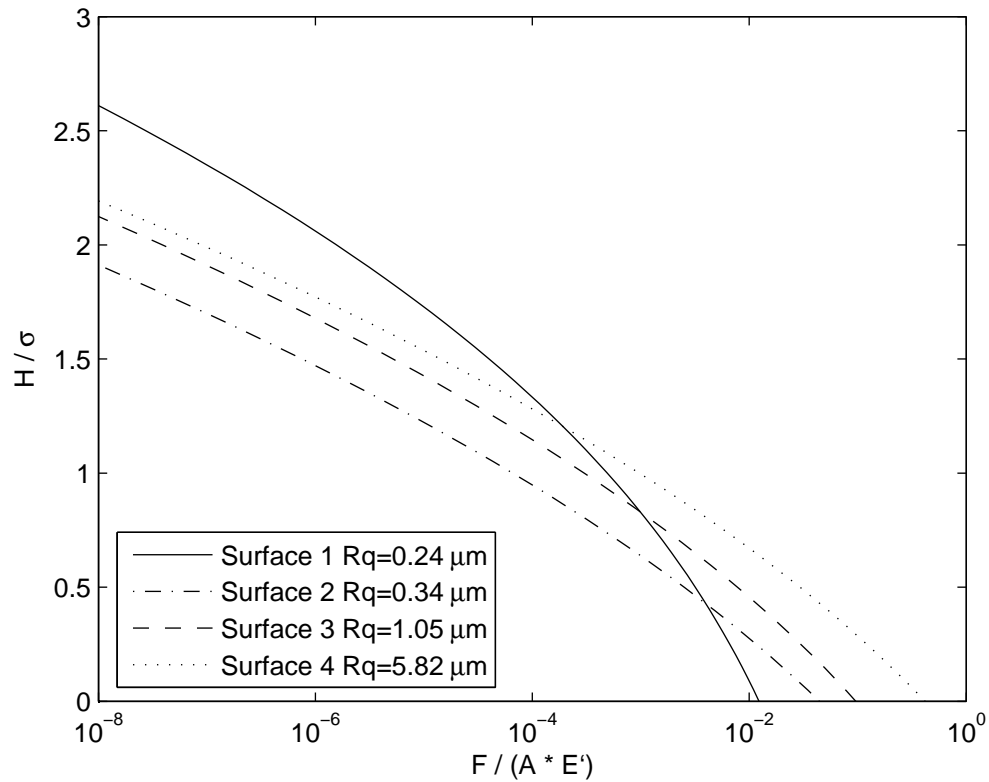


Figure 6.18: Surface Separation as a function of dimensionless load for surfaces of different roughness modeled using the GW statistical method for perfectly elastic material deformation.

Figs. 6.15-6.18 show some interesting results when considering different surface roughness values. All of the models show the ranking behavior seen in the area calculations above but only for very high loads when the surfaces reach zero separation. Aside from this phenomenon, there appears to be very little definitive effect of roughness on separation since the separation models appear to be fairly random. The qualitative trends are the same for all the modeling techniques and roughness but there seems to be little order due to roughness. This is especially true for the multiscale model results

shown in Figs. 6.15-6.16. However, the statistical models, whose results are shown in Figs. 6.17-6.18, do display the ranking behavior with the smoother surfaces having a decreased surface separation except for the smoothest surfaces which behaves independently of the others including a unique slope. When recalling the similarities among the area calculations this seems to be quite strange behavior. Also note that each modeling technique requires a unique load range to reach full contact or zero separation.

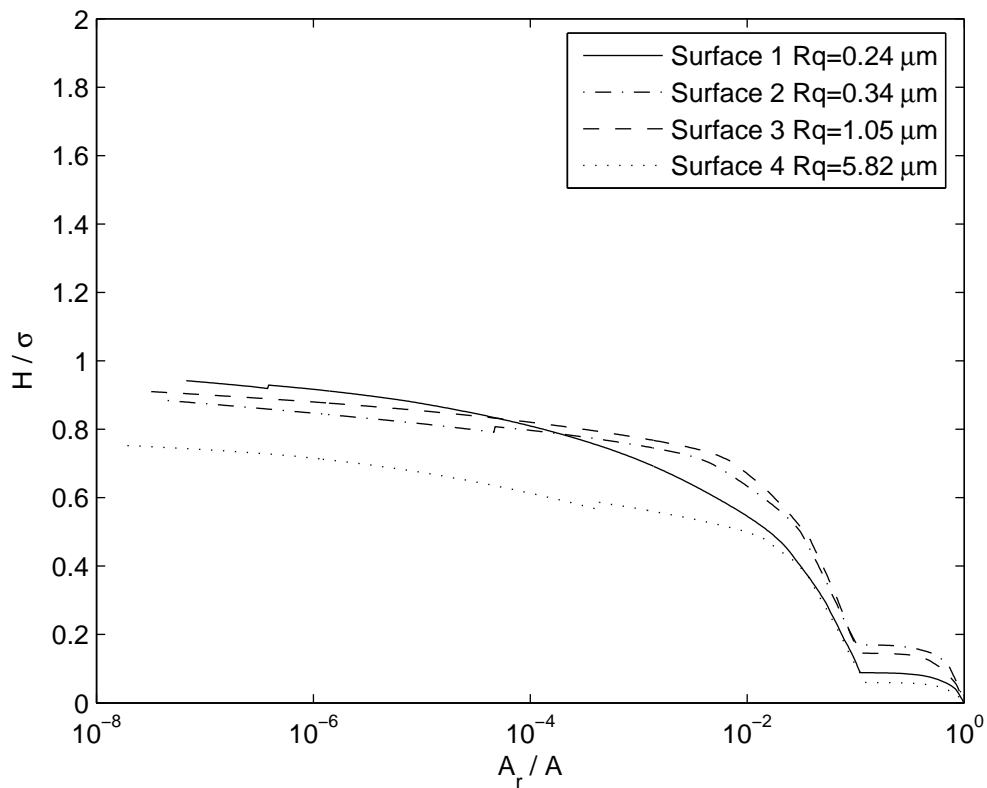


Figure 6.19: Surface separation as a function of real area of contact for surfaces of different roughness modeled using the sinusoidal based multiscale method for elastic-plastic material deformation.

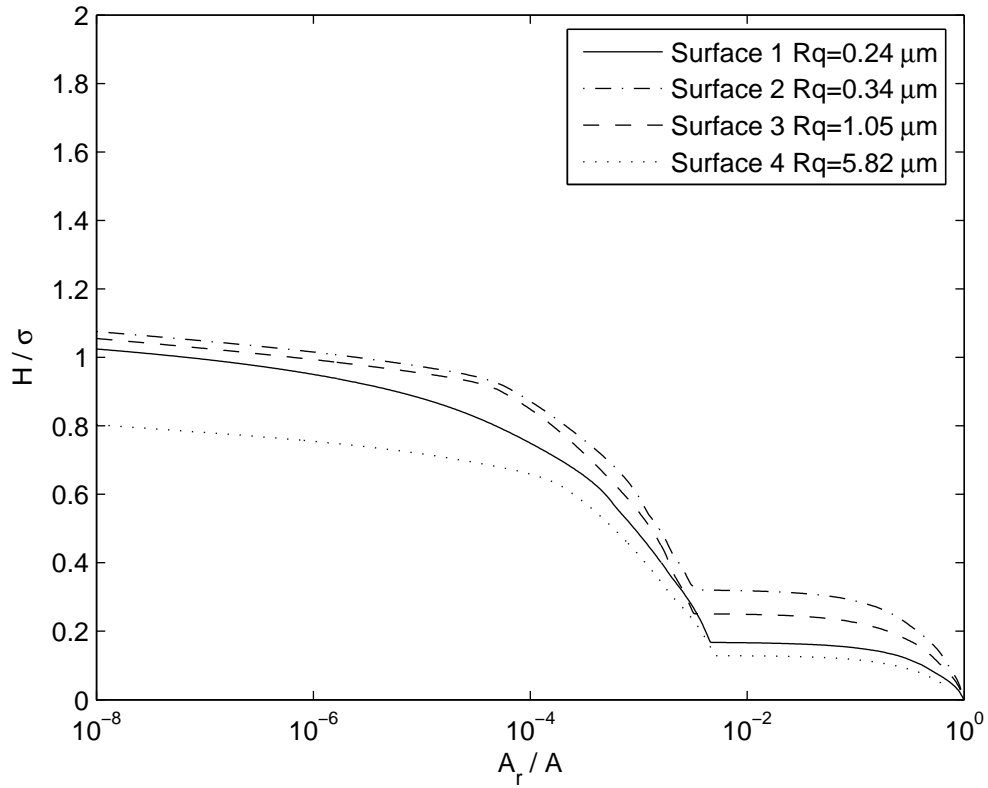


Figure 6.20: Surface separation as a function of real area of contact for surfaces of different roughness modeled using the sinusoidal based multiscale method for perfectly elastic material deformation.

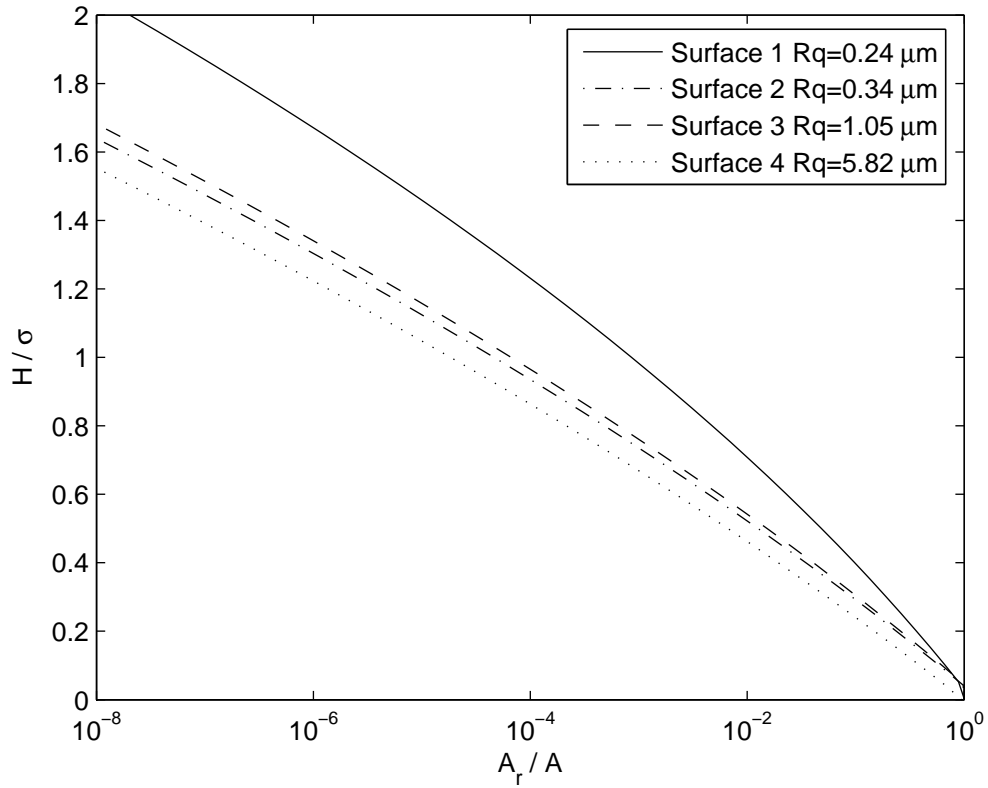
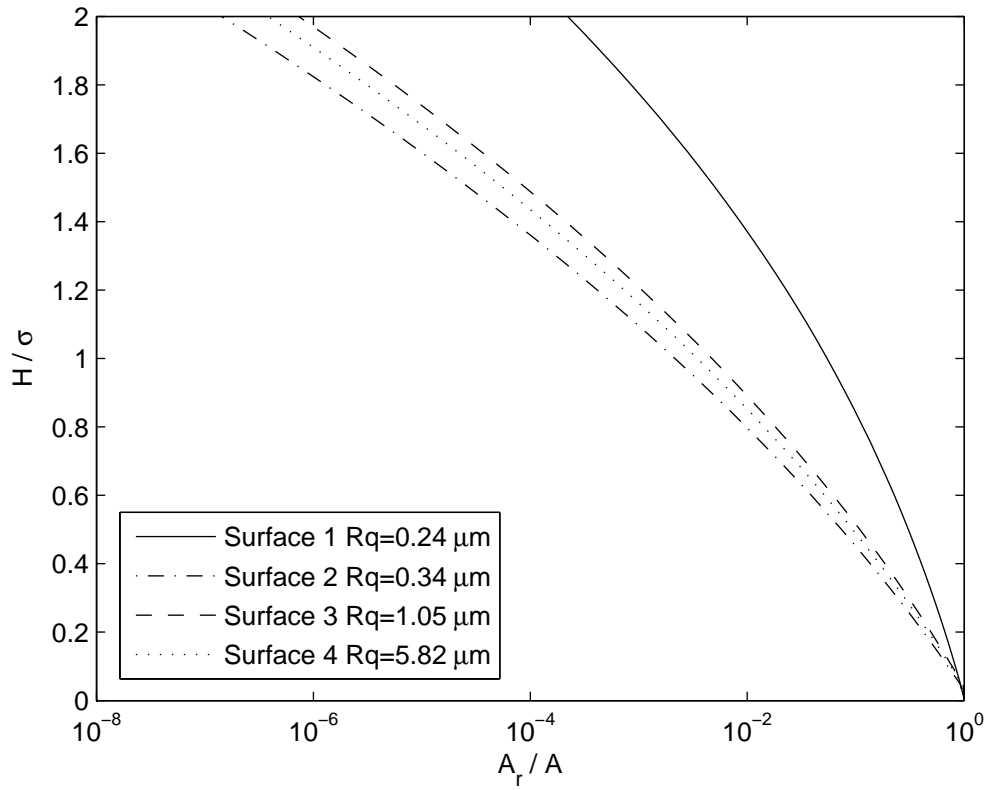


Figure 6.21: Surface separation as a function of real area of contact for surfaces of different roughness modeled using the JG statistical method for elastic-plastic material deformation.



Fi

Figure 6.22: Surface separation as a function of real area of contact for surfaces of different roughness modeled using the GW statistical method for perfectly elastic material deformation.

Surface	1	2	3	4
Roughness	0.24 μm	0.34 μm	1.05 μm	5.82 μm
β for GW model	153.7	5.2	8.8	6.8
β for JG model	159.9	10.02	14.2	12.8

Table 6.3: Rough Surface Characteristics and Adjusted Separation Values (Eq. 4.54).

Figures 6.19-6.22 also have no ranking behavior. Recall that the statistical results (Figs. 6.17, 6.18, 6.21, & 6.22) all feature the adjusted surface separation technique with great success since all the cases show zero surface separation when the contact area has reached one which is equivalent to full contact for the non-dimensional techniques displayed in Figs. 6.21-6.22. The values of β in Eq. 4.54 are vastly different for each roughness with no apparent correlation between these values and the roughness itself as seen in Table 6.3. The β -values are all reasonable with the exception of the smoothest surface. As mentioned previously, a presumably acceptable β -value lies between 4 and 12. If β equals 12, then the adjustment seen in Eq. 4.54 relates to $\pm 6\sigma$. Statistical analysis will show that this value will include 99.7% of the asperities. Therefore, the values for the smoothest surface seem quite extreme with no obvious explanation. Future work in this area will be necessary to explain this discrepancy.

6.4.3 Electrical Contact Resistance

In this section, the results for the electrical contact resistance (ECR) are compared for the four different rough surfaces used in this work. As before, the results are given with the units of Ohms (Ω) for the ECR along the y-axis and non-dimensional load along the x-axis.

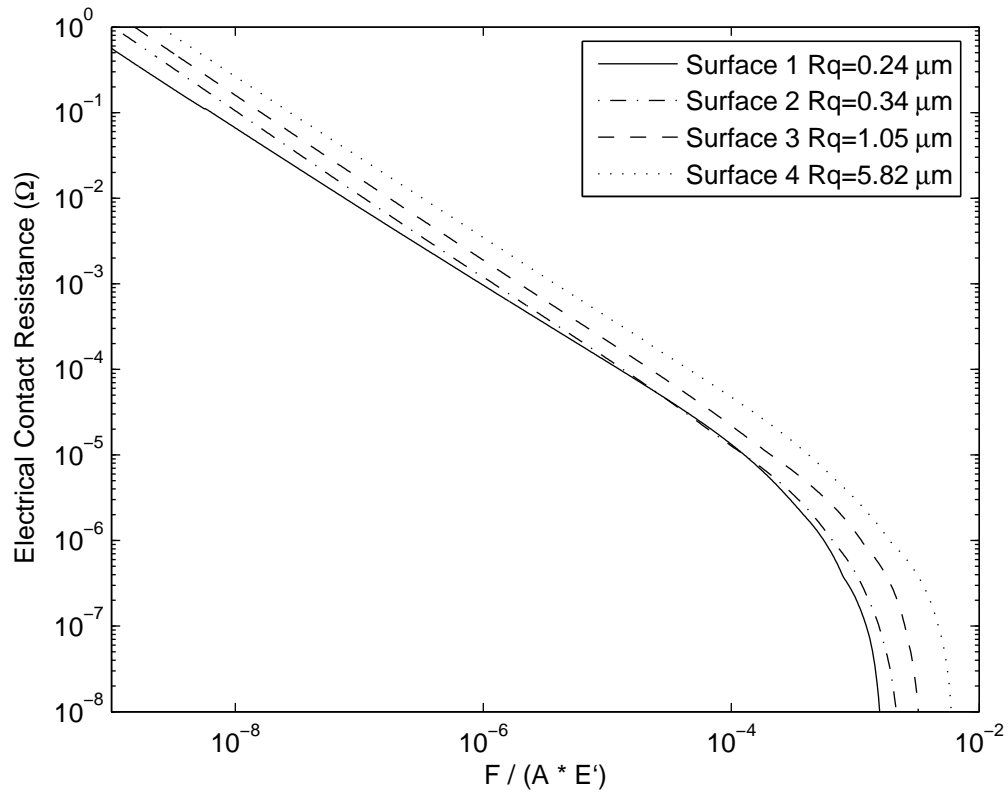
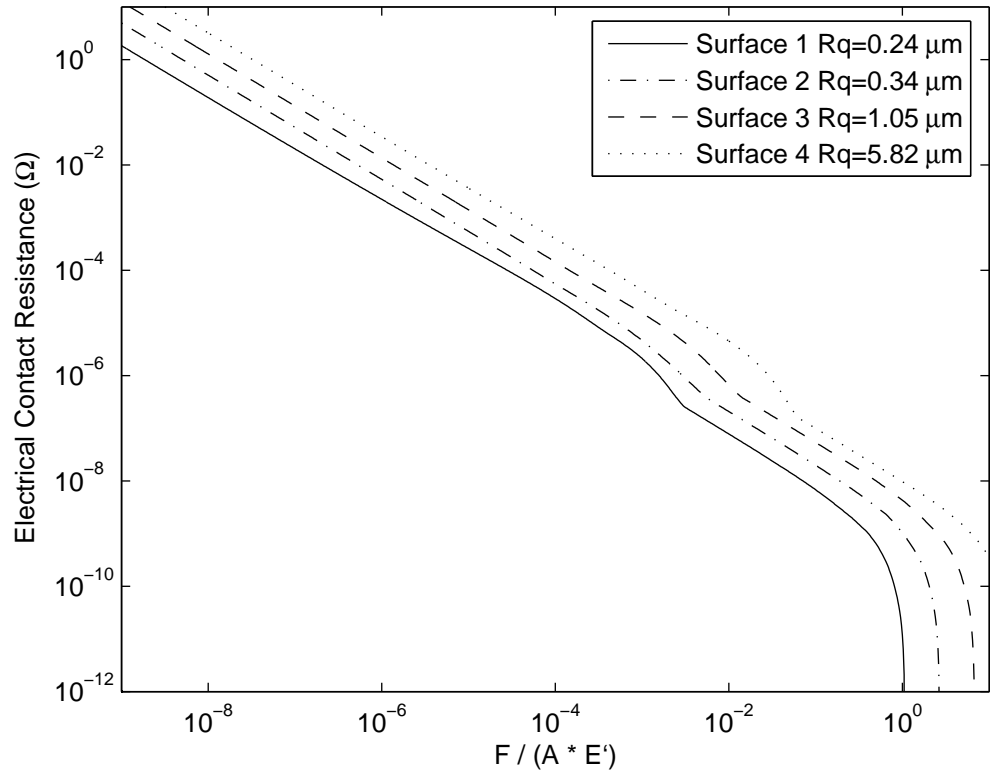
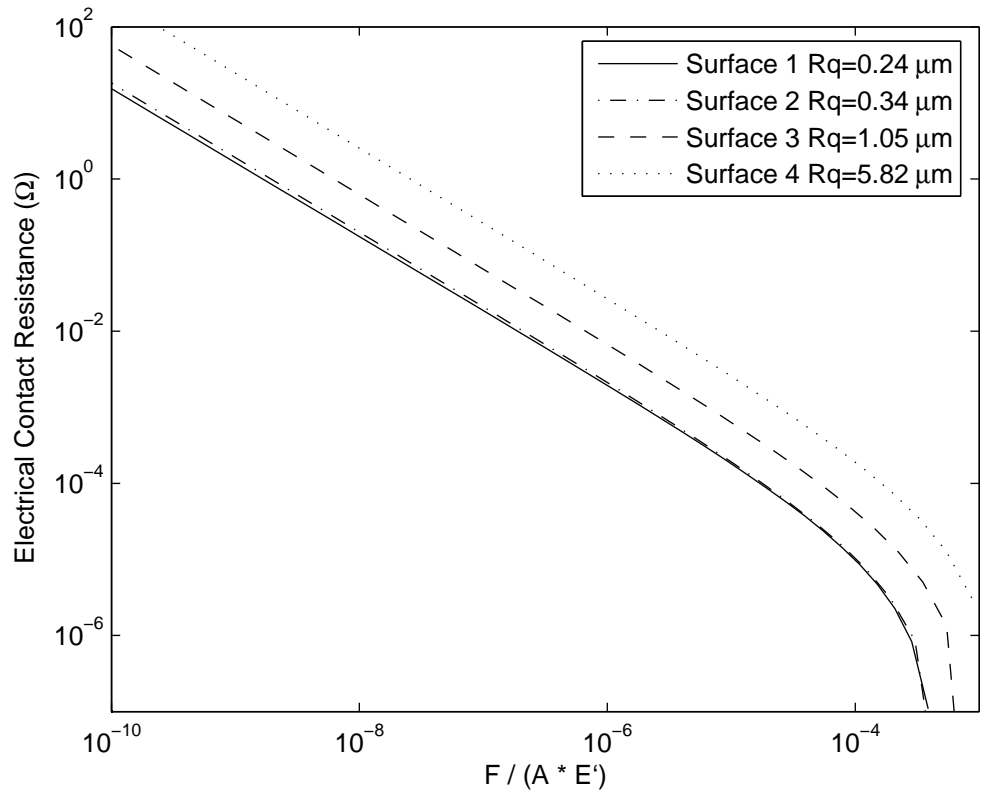


Figure 6.23: Electrical contact resistance (ECR) as a function of dimensionless load for surfaces of different roughness modeled using the sinusoidal based multiscale method for elastic-plastic material deformation.



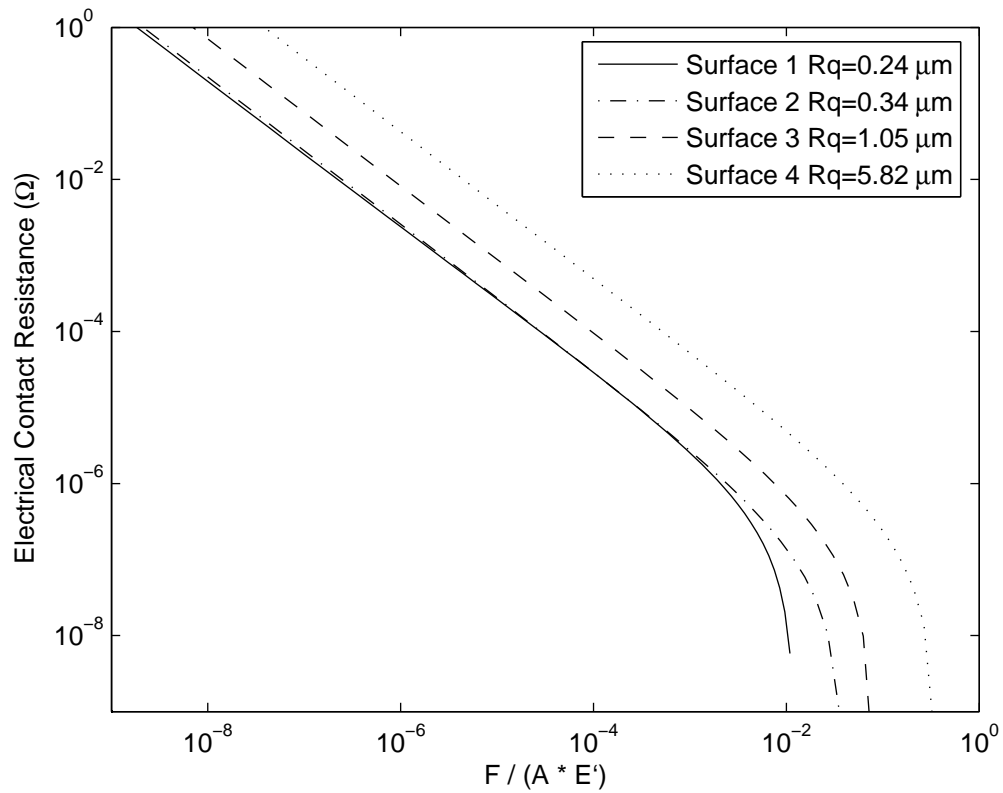
Fi

Figure 6.24: Electrical contact resistance (ECR) as a function of dimensionless load for surfaces of different roughness modeled using the sinusoidal based multiscale method for perfectly elastic material deformation.



Fi

Figure 6.25: Electrical contact resistance (ECR) as a function of dimensionless load for surfaces of different roughness modeled using the JG statistical method for elastic-plastic material deformation.



Fi

Figure 6.26: Electrical contact resistance (ECR) as a function of dimensionless load for surfaces of different roughness modeled using the GW statistical method for elastic-plastic material deformation.

In accordance with the real area of contact, electrical contact resistance is very similar for the four surfaces and is also ranked according to roughness with the smoothest surface having the least resistance values, seen in Figs. 6.23-6.26. The different modeling techniques have already been established to show qualitatively similar trends for a common surface. However, the behavior of the four different models for the various roughnesses is strikingly dissimilar. The overall decreasing trend with a sudden drop is common, but the multiscale models (Figs. 6.23-6.24) react to each roughness with a

nearly equidistant gap. In comparison, the two statistical models (Figs. 6.25-6.26) show no gap for all but high loads for the smoothest surfaces but rather large gaps for the higher roughness values. There is also a strange shoulder in the multiscale perfectly elastic solution (Fig. 6.24) which is not present in the other models. However, the shoulder seems to be at nearly the same location when the multiscale elastic-plastic model (Fig. 6.23) shows the sudden drop in resistance for the very high loads. This may be due to the discrete scales flattening out at higher loads. Since the perfectly elastic contact cannot behave in this manner the next iteration requires the surface to return to nearly linear behavior till much higher loads.

6.4.4 Thermal Contact Resistance

This section will display the results for the thermal contact resistance calculations when considering varied surface roughness. This comparison is done for each model in order to show further distinction among their unique mathematical methods. It is important to note that the following results are for thermal contact resistance without the scale-dependent surface characteristics included. It is seen in the earlier thermal conductivity comparison that scale-dependency has negligible effects on most models, loads, and deformation characteristics and has therefore been omitted from these comparisons. The units used for these comparisons are Kelvin meters squared per Watt along the y-axis (TCR) and non-dimensional load along the x-axis.

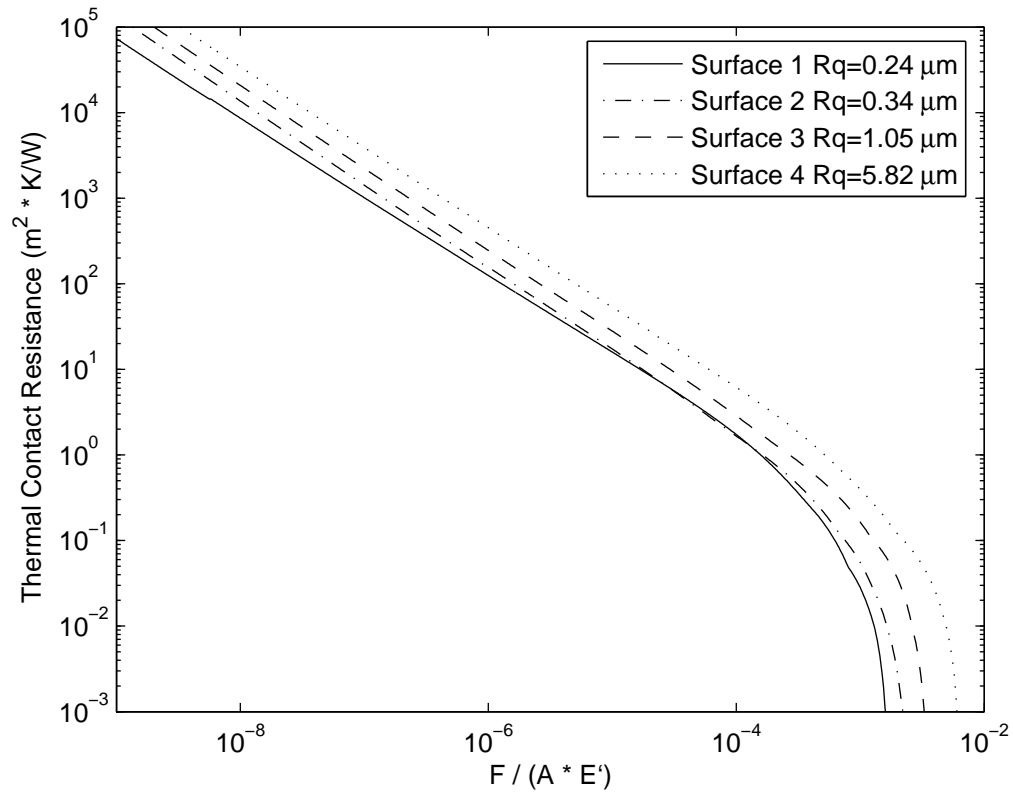
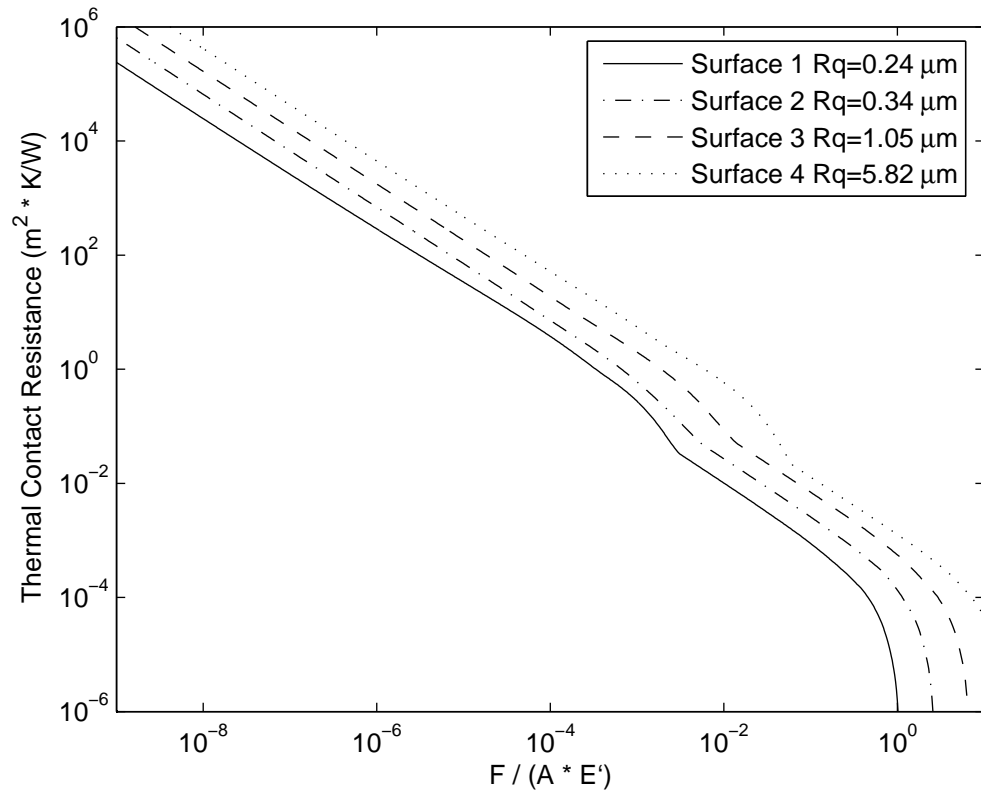
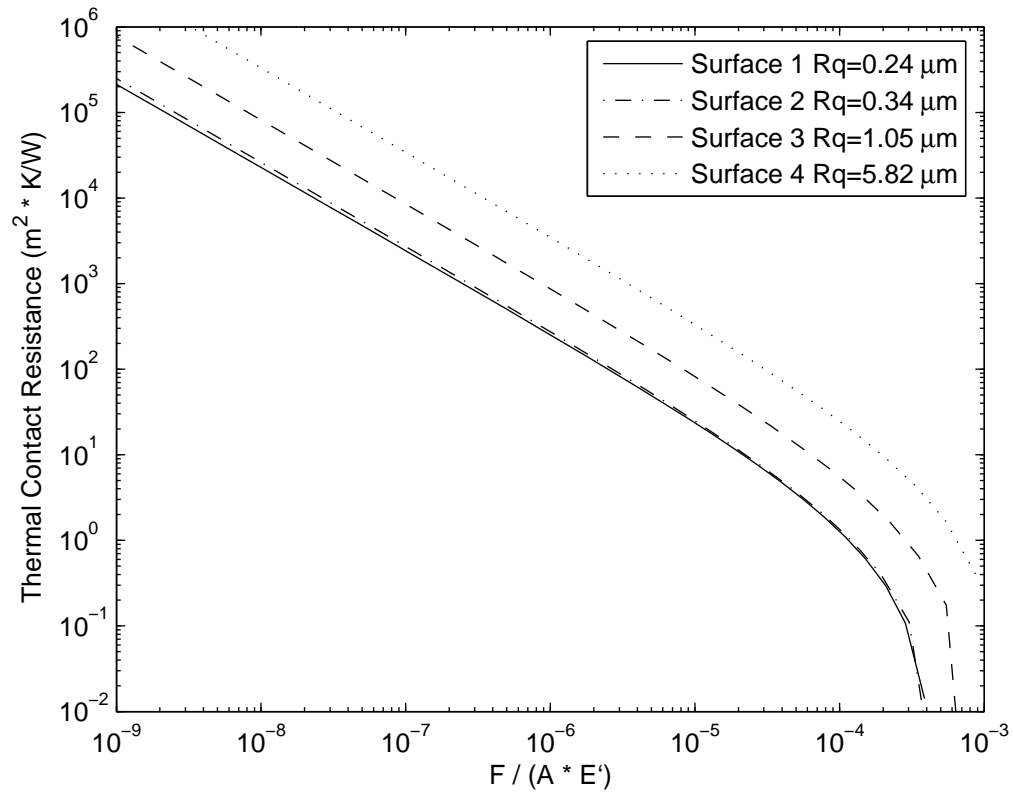


Figure 6.27: Thermal contact resistance (TCR) as a function of dimensionless load for surfaces of different roughness modeled using the sinusoidal based multiscale method for elastic-plastic material deformation.



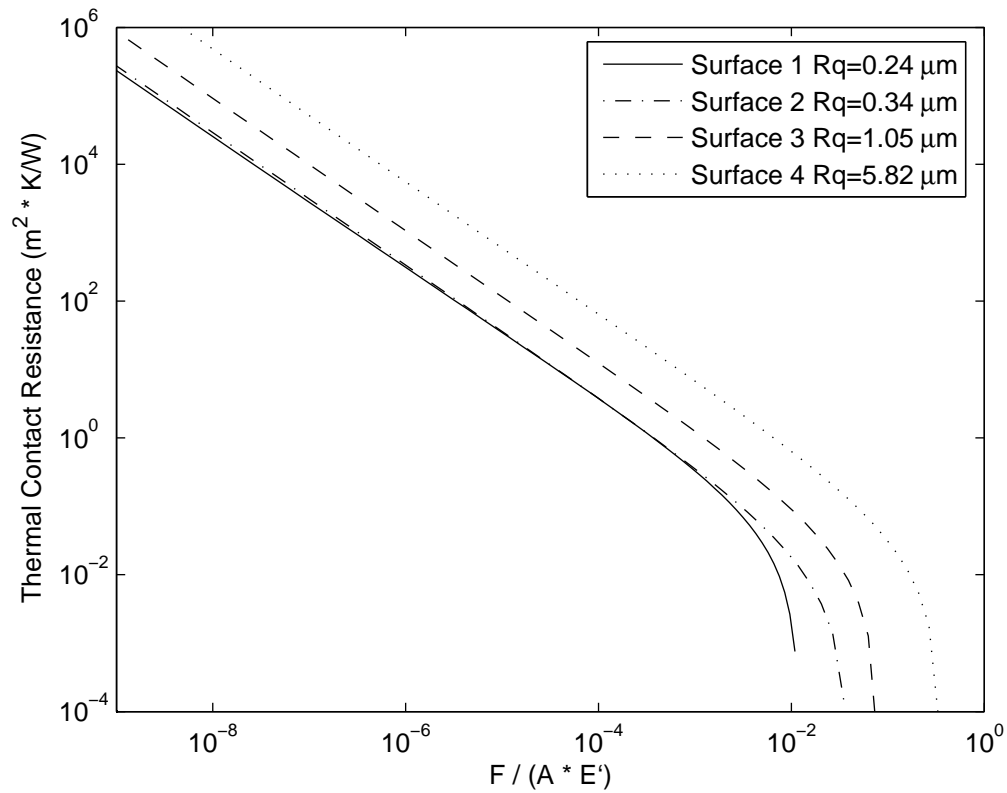
Fi

Figure 6.28: Thermal contact resistance (TCR) as a function of dimensionless load for surfaces of different roughness modeled using the sinusoidal based multiscale method for perfectly elastic material deformation.



Fi

Figure 6.29: Thermal contact resistance (TCR) as a function of dimensionless load for surfaces of different roughness modeled using the JG statistical method for elastic-plastic material deformation.



Fi

Figure 6.30: Thermal contact resistance (TCR) as a function of dimensionless load for surfaces of different roughness modeled using the GW statistical method for perfectly elastic material deformation.

Figures 6.27-6.30 display the results of thermal contact resistance (TCR) for each different model with the intent of comparing how each model reacts to a change of surface roughness. At first glance, all the models appear to give the same or at least extremely similar results. Indeed, all the models show a steady, nearly linear, decreasing trend for the majority of loads with a sudden drop for the higher loads. However, upon closer inspection, TCR for the elastic-plastic models, Figs. 6.27 & 6.29, terminates at significantly lower loads than the perfectly elastic models, Figs. 6.28 & 6.30. Also, the

TCR models show shoulders for only the multiscale perfectly elastic case very near the values at which the multiscale elastic-plastic model drops suddenly for the higher loads. This correlates well with the electrical contact resistance since the calculations for both effects are very similar. The same ranking behavior is seen here as in the previous calculations but the multiscale models show an almost uniform change from one roughness to another. Specifically, the multiscale elastic-plastic model, Fig. 6.27, shows, for the most part, equal but small gaps between the four surfaces. The statistical models seem to be much more sensitive to roughness changes since these models show almost no gap between the two very smooth surfaces (surfaces 1 & 2, 0.24 and 0.34 μm roughness respectively) with a considerably larger jump in the between the remaining surfaces. Note that the results for ECR and TCR are all quantitatively similar for both models and all surface roughnesses.

CHAPTER 7

CONCLUSIONS

The results from a multiscale model based on stacked sinusoidal surfaces have shown to be qualitatively similar in comparison with existing statistical contact models. When viewing surface separation as a function of dimensionless load, it seems that the multiscale models offer a differing description of how the surface behaves. At high loads, the multiscale methods predict no separation between the surfaces which correlates exactly with the area of contact equaling the apparent area of contact (complete contact). However, even though the statistical methods show a similar trend as the maximum area is reached, there appears to still be some separation between the two surfaces. This is most likely a result of the statistical methods being designed more for lightly loaded contacts and ignoring the change in overall peak to valley height between asperities at higher loads. The adjusted statistical model separation calculation offered in this work takes this effect into account and does show zero separation at the maximum contact area. Electrical contact resistance predictions seem reasonable based on the similarity between statistical and multiscale methods. Actually, the statistical and multiscale models predict very similar values, while the predicted contact areas are not as similar. This suggests that using contact resistance measurements may not be an effective way of evaluating rough surface contact models.

In response to concerns about the convergence of the multiscale techniques, this work relates a power fit to the FFT data which reveals that the sinusoidal multiscale technique will converge as long as the average pressure (proportional to amplitude) stays constant or decreases as the wavelength decreases. This situation requires that the exponent in the power fit remain 1 or greater for the multiscale sinusoidal technique to converge.

Finally, the multiscale sinusoidal method is used to generate results for a variety of real surfaces shows the overall expected trends for area, electrical contact resistance and surface separation. As is expected, the results for the surfaces are ranked according to roughness yet produce extremely similar results. Upon first inspection, it appears that surface separation does not match the ranking behavior for the various surfaces. However, at greater loads, lower roughness values do decrease surface separation.

BIBLIOGRAPHY

1. Greenwood, J.A. and J.B.P. Williamson, *Contact of Nominally Flat Surfaces*. Proc. R. Soc. Lond. A, 1966(295): p. 300-319.
2. Chang, W.R., I. Etsion, and D.B. Bogy, *An Elastic-Plastic Model for the Contact of Rough Surfaces*. ASME J. Tribol., 1987. 109(2): p. 257-263.
3. Jackson, R.L. and I. Green, *A Statistical Model of Elasto-plastic Asperity Contact between Rough Surfaces*. Trib. Int., 2006. 39(9): p. 906-914.
4. Kogut, L. and I. Etsion, *A Finite Element Based Elastic-Plastic Model for the Contact of Rough Surfaces*. Tribology Transactions, 2003. 46(3): p. 383-390.
5. Kogut, L., and Jackson, R. L., *A Comparison of Contact Modeling Utilizing Statistical and Fractal Approaches*. ASME J. Tribol., 2005. 128(1): p. 213-217.
6. Majumdar, A. and B. Bhushan, *Fractal Model of Elastic-plastic Contact Between Rough Surfaces*. ASME J. of Tribol., 1991. 113(1): p. 1-11.
7. Wang, S., J. Shen, and W.K. Chen. *Determination of the Fractal Scaling Parameter from Simulated Fractal Regular Surface Profiles Based on the Weierstrass-Mandelbrot Function (IJTC2006-12068)*. in *STLE/ASME Int. Joint Trib. Conf.* 2006. San Antonio, TX.
8. Yan, W. and K. Komvopoulos, *Contact Analysis of Elastic-Plastic Fractal Surfaces*. Journal of Applied Physics, 1998. 84(7): p. 3617-3624.
9. Bora, C.K., et al., *Multiscale Roughness and Modeling of MEMS Interfaces*. Tribology Letters, 2005. 19(1): p. 37-48.
10. Ciavarella, M., et al., *Linear Elastic Contact of the Weierstrass Profile*. Proc. R. Soc. Lond. A, 2000. 1994(456): p. 387-405.
11. Jackson, R.L. and J.L. Streater, *A Multiscale Model for Contact between Rough Surfaces*. Wear, 2006. 261(11-12): p. 1337-1347.
12. Fleck, N.A. and J.W. Hutchinson, *A Phenomenological Theory for Strain Gradient Effects in Plasticity*. J. Mech. Phys. Solids, 1993(41): p. 1825-1857.

13. Wei, Y. and J.W. Hutchinson, *Hardness Trends in Micron Scale Indentation*. J. Mech. Phys. Solids, 2003(51): p. 2037-2056.
14. Fleck, N.A., et al., *Strain Gradient Plasticity: Theory and Experiment*. Acta Metall. Mater., 1994. 42(2): p. 475-487.
15. Gao, H., et al., *Mechanism-Based Strain Gradient Plasticity-I. Theory*. J. Mech. Phys. Solids, 1999(47): p. 1239-1263.
16. Gao, H., et al., *Mechanism-Based Strain Gradient Plasticity- II. Analysis*. J. Mech. Phys. Solids, 2000(48): p. 99-128.
17. Johnson, K.L., *Contact Mechanics*. 1985, Cambridge, U.K.: Cambridge University Press. 452.
18. Jackson, R.L. and I. Green, *A Statistical Model of Elasto-Plastic Asperity Contact Between Rough Surfaces*. Tribology Int., 2006(39): p. 906-914.
19. Chang, W.R., I. Etsion, and D.B. Bogy, *An elastic-plastic model for the contact of rough surfaces*. ASME J. Tribol., 1987. 109: p. 257-63.
20. Kogut, L. and I. Etsion, *Elastic-plastic contact analysis of a sphere and a rigid flat*. J. App. Mech. Trans. ASME, 2002. 69(5): p. 657-62.
21. Majumdar, A. and B. Bushnan, *Fractal Model of Elastic-Plastic Contact Between Rough Surfaces*. ASME J. Tribol., 1991. 113(1): p. 1-11.
22. Archard, J.F., *Elastic Deformation and the Laws of Friction*. Proc. R. Soc. Lond. A, 1957(243): p. 190-205.
23. Johnson, K.L., J.A. Greenwood, and J.G. Higginson, *The Contact of Elastic Regular Wavy Surfaces*. Int. J. Mech. Sci., 1985. 27(6): p. 383-396.
24. Krithivasan, V. and R.L. Jackson, *An Analysis of Three-Dimensional Elasto-Plastic Sinusoidal Contact*. Tribology Letters, 2007. 27(1): p. 31-43.
25. Jackson, R.L., V. Krithivasan, and W.E. Wilson, *The Pressure to Cause Complete Contact between Elastic Plastic Sinusoidal Surfaces*. IMechE J. of Eng. Trib. - Part J. In Print.
26. McCool, J.I., *Comparison of Models for the Contact of Rough Surfaces*. Wear, 1986(107): p. 37-60.
27. Front, I., *The Effects of Closing Force and Surface Roughness on Leakage in Radial Face Seals*, in *Israel Institute of Technology*. 1990, Technion.

28. Jackson, R.L. and I. Green, *A Finite Element Study of Elasto-Plastic Hemispherical Contact*. ASME J. Tribol., 2005. 127(2): p. 343-354.
29. Holm, R., *Electric Contacts*. 4th ed. 1967, New York: Springer Verlag. 21.
30. Madhusudana, C.V., *Thermal Contact Conductance*. 1996, New York: Springer-Verlag.
31. Cooper, M.G., B.B. Mikic, and M.M. Yovanovich, *Thermal Contact Conductance*. Int. J. Heat Mass Transfer, 1969(12): p. 279-300.
32. Jackson, R.L., S.H. Bhavnani, and T.P. Ferguson, *A Multi-scale Model of Thermal Contact Resistance between Rough Surfaces*. ASME J. Heat Transfer, 2007.
33. Kogut, L. and I. Etsion, *Electrical Conductivity and Friction Fore Estimation in Compliant Electrical Connectors*. STLE Tribol. Trans., 2000. 43(4): p. 816-822.
34. Prasher, R.S. and P.E. Phelan, *Microscopic and Macroscopic Thermal Contact Resistances of Pressed Mechanical Contacts*. J. App. Phys., 2006(100).
35. Ciavarella, M., et al., *Linear elastic contact of the Weierstrass Profile*. Proc. R. Soc. Lond. A, 2000(456): p. 387-405.
36. Drinkwater, B.W., R.S. Dwyer-Joyce, and P. Cawley. *A Study of the Interaction between Ultrasound and a Partially Contacting Solid--Solid Interface*. in *Mathematical, Physical and Engineering Sciences*. 1996: The Royal Society.